Dual function of perivascular fibroblasts in vascular stabilization in zebrafish

Arsheen M. Rajan[1], Roger C. Ma[1], Katrinka M. Kocha[1], Dan J. Zhang[2], and Peng Huang[1]*

[1] Department of Biochemistry and Molecular Biology, Cumming School of Medicine, Alberta Children's Hospital Research Institute, University of Calgary, 3330 Hospital Drive, Calgary, Alberta, Canada T2N 4N1

[2] Department of Biological Sciences, University of Calgary, 2500 University Drive, Calgary, Alberta, Canada T2N 1N4

* Correspondence should be addressed to PH.

Email: huangp@ucalgary.ca

Tel: 403-220-4612

Running title: Perivascular fibroblasts in vascular stabilization

Keywords: Perivascular fibroblast, Pericyte, Sclerotome, Collagen, Extracellular matrix, Zebrafish

ABSTRACT

Blood vessels are vital to sustain life in all vertebrates. While it is known that mural cells (pericytes and smooth muscle cells) regulate vascular integrity, the contribution of other cell types to vascular stabilization has been largely unexplored. Using zebrafish, we identified sclerotome-derived perivascular fibroblasts as a novel population of blood vessel associated cells. In contrast to pericytes, perivascular fibroblasts emerge early during development, express the extracellular matrix (ECM) genes *col1a2* and *col5a1*, and display distinct morphology and distribution. Time-lapse imaging reveals that perivascular fibroblasts serve as pericyte precursors. Genetic ablation of perivascular fibroblasts results in dysmorphic blood vessels with variable diameters. Strikingly, *col5a1* mutants show spontaneous hemorrhage, and the penetrance of the phenotype is strongly enhanced by the additional loss of *col1a2*. Together, our work reveals dual roles of perivascular fibroblasts in vascular stabilization where they establish the ECM around nascent vessels and function as pericyte progenitors.

AUTHOR SUMMARY

Blood vessels are essential to sustain life in humans. Defects in blood vessels can lead to serious diseases, such as hemorrhage, tissue ischemia, and stroke. However, how blood vessel stability is maintained by surrounding support cells is still poorly understood. Using the zebrafish model, we identify a new population of blood vessel associated cells termed perivascular fibroblasts, which originate from the sclerotome, an embryonic structure that is previously known to generate the skeleton of the animal. Perivascular fibroblasts are distinct from pericytes, a known population of blood vessel support cells. They become associated with blood vessels much earlier than pericytes and express several collagen genes, encoding main components of the extracellular matrix. Loss of perivascular fibroblasts or mutations in collagen genes result in fragile blood vessels prone to damage. Using cell tracing in live animals, we find that a subset of perivascular fibroblasts can differentiate into pericytes. Together, our work shows that perivascular fibroblasts play two important roles in maintaining blood vessel integrity. Perivascular fibroblasts secrete collagens to stabilize newly formed blood vessels and a sub-population of these cells also functions as precursors to generate pericytes to provide additional vascular support.

INTRODUCTION

The vascular system is crucial to the survival of vertebrates. Blood vessels must rapidly expand and contract in response to systemic cues, but also maintain the stability to withstand the stress of blood flow. To maintain their integrity, blood vessels are supported by a highly specialized perivascular architecture comprised of blood vessel associated cells and the surrounding extracellular matrix (ECM) (1,2). Compromised vascular integrity can result in devastating human diseases, such as aneurysms, vascular malformations, and hemorrhagic strokes (3-6). However, how blood vessels are stabilized by different perivascular components is still poorly understood.

The prevailing model is that vascular stability is maintained at three different levels: endothelial cells, mural cells and the surrounding ECM (2). First, blood vessels are lined by endothelial cells. Adherens and tight junctions between endothelial cells provide the primary barrier to passage of fluids, cells, and macromolecules between blood and tissues (7). Second, vascular smooth muscle cells (vSMCs) and pericytes, collectively known as mural cells, closely interact with and stabilize the endothelium (8). vSMCs form a continuous protective sheath around large diameter blood vessels, whereas pericytes are solitary cells partially covering smaller blood vessels such as capillaries. Defects in mural cell specification or recruitment result in widespread vascular leakage and early lethality in mice (9-13). Lastly, the vascular ECM provides structural support for blood vessels (1,14). Mutations in ECM proteins, such as collagens and laminins, lead to early death due to blood vessel rupture in mice (15-18). In humans, defects in fibril forming collagens (type I, III and V), as well as molecules involved in collagen modification and processing, have been associated with Ehlers-Danlos syndrome (EDS) (19). EDS patients are characterized by a significant vascular fragility that often leads to spontaneous rupture of blood vessel walls. Thus, work in both animal models and human patients shows the importance of collagen in maintaining vascular stability. However, one unresolved question is how newly formed blood vessels are stabilized in the early time window before the differentiation of mural cells.

vSMCs and pericytes are the most well-studied blood vessel associated cells and are classically defined by the expression of alpha smooth muscle actin (ACTA2) and platelet-derived growth factor receptor b (PDGFRb), respectively (20,21). Lineage tracing in mice and chick-quail chimeras demonstrate a heterogeneous developmental origin of mural cells (20-23). For example, vSMCs covering the trunk aorta originate from either the neural crest or the sclerotome of the somite, depending on the axial position. Other than mural cells, several types of perivascular cells have been identified, including adventitial cells (24), fibroblasts (25), immune cells (26-28), and astrocytes (29). However, whether these different cell types play roles in vascular stabilization is unknown.

Recent single cell transcriptional profiling studies in mice have revealed the presence of perivascular fibroblast-like cells in the adult mouse brain that are not labeled by classical mural cell markers (30-33). In contrast to mural cells, perivascular fibroblast-like cells adhere loosely to blood vessels and show robust expression of many ECM components, such as collagens. Previous studies have described similar cell populations in the mouse central nervous system that contribute to fibrotic scar formation after injury (34–37). However, where these perivascular fibroblast-like cells originate from during development and how they regulate blood vessel development and stabilization have not been explored.

Zebrafish is a powerful model to study human cardiovascular diseases (38-41). The organization, development and function of the vasculature, including mural cells, are highly conserved between zebrafish and mammals (38,42,43). In the zebrafish trunk, intersegmental vessels (ISVs) sprout from the dorsal aorta (DA) at around 24 hpf (hours post fertilization) and fully establish the metameric pattern by 36 hpf (44). Interestingly, pericytes, the primary mural cells along the ISVs, only emerge at 60 hpf (45). This raises the question how nascent blood vessels are stabilized prior to the differentiation of pericytes. In our work, we describe a novel population of collagen-expressing perivascular fibroblasts that become closely associated with ISVs soon after vessel formation. Perivascular fibroblasts originate from the sclerotome and are distinct from pericytes in their morphology, distribution, and marker expression. Using a combination of *in vivo* live imaging, genetic ablation and CRISPR mutant analysis, we demonstrate that perivascular fibroblasts play dual roles in stabilizing nascent ISVs by regulating the vascular ECM and later functioning as pericyte progenitors. Together, our work provides important insights into the development of perivascular support structures and suggests a molecular and cellular basis of Ehlers-Danlos syndrome.

RESULTS

Perivascular fibroblasts express several collagen genes

We previously developed a sclerotome-specific transgenic line *nkx3.1:Gal4; UAS:Nitroreductase-mCherry* (*nkx3.1*$^{NTR\text{-}mCherry}$, similar designations are used for all Gal4/UAS transgenic lines in this paper) (46). This reporter labels the initial sclerotome domains as well as their descendants due to the perdurance of the mCherry protein. Examination of the *nkx3.1*$^{NTR\text{-}mCherry}$ line in combination with an endothelial reporter, *kdrl:EGFP*, revealed that a population of mCherry^{+} cells was closely associated with intersegmental vessels (ISVs) at 48 hpf (Fig. 1A). This result suggests that the sclerotome contributes to a population of perivascular cells well before the appearance of pericytes at 60 hpf (45). Interestingly, *nkx3.1*$^{NTR\text{-}mCherry}$-expressing perivascular cells at 52 hpf were also labeled by a pan-fibroblast reporter, *col1a2:GFP* (46) (Fig. 1B). Consistent with this result, fluorescent in situ hybridization showed that ISV-associated perivascular cells co-expressed several ECM genes, including *col1a2* (*collagen 1a2*) and *col5a1* (*collagen 5a1*) at 48 hpf (Fig. 1C and S1). These collagen-expressing perivascular cells are reminiscent of perivascular fibroblast-like cells recently identified in the adult mouse brain by single cell RNA sequencing (Marques et al., 2016; Saunders et al., 2018; Vanlandewijck et al., 2018; Zeisel et al., 2018). We therefore refer to this population of collagen-expressing ISV-associated cells as 'perivascular fibroblasts'.

Perivascular fibroblasts originate from the sclerotome

The expression of *nkx3.1*$^{NTR\text{-}mCherry}$ in perivascular fibroblasts suggests that the sclerotome is the embryonic source of these cells. We have previously shown that the sclerotome in zebrafish has a bipartite organization with a ventral domain and a smaller dorsal domain (46). The ventral sclerotome domain further gives rise to a population of notochord associated cells. At 24 hpf, the sclerotome consists of three compartments: the dorsal sclerotome domain, the ventral sclerotome domain, and notochord associated cells derived from the ventral domain (Fig. 2A). To determine the contribution of these three compartments to perivascular fibroblasts, we performed confocal time-lapse imaging in *nkx3.1*$^{NTR\text{-}mCherry}$*; kdrl:EGFP* embryos. The *nkx3.1*$^{NTR\text{-}mCherry}$ reporter labels sclerotome progenitors and their progeny, while the endothelial specific *kdrl:EGFP* line allows us to visualize the ISVs. The trunk region of embryos (somite 12-18) was imaged laterally at 6-9 minute intervals starting at 25 hpf, immediately after the emergence of ISV sprouts (Fig. 2B and Movie S1). At 30 hpf, most ISVs became visibly lumenized. During ISV sprouting and lumenization, mCherry^{+} cells can be observed associated with the *kdrl:EGFP*-labeled endothelium (Fig. 2B and S2; Movie S1). By the end of the movie at 49.5 hpf, mCherry^{+} perivascular fibroblasts 'decorated' the entire ISVs along the dorsal-ventral (D-V) axis.

By retrospective cell tracing, we showed that perivascular fibroblasts can be traced to all three compartments of the sclerotome. Of 170 perivascular fibroblasts traced, 28 cells originated from the dorsal sclerotome domain (16%), 112 from the ventral sclerotome domain (66%), and 30 from notochord associated cells (18%). Since notochord associated cells are derived from the ventral sclerotome domain, this result suggests that the ventral sclerotome is the main contributor of perivascular fibroblasts (142/170 cells, 84%).

To better compare the contribution of sclerotome progenitors from different compartments, we subdivided perivascular fibroblasts into two domains based on their final D-V positions along the ISVs. The position of the horizontal myoseptum was used as a landmark to define perivascular fibroblasts at dorsal or ventral ISVs (Fig. 2A). The 170 perivascular fibroblasts can be traced back to 122 sclerotome progenitors. These sclerotome progenitors typically underwent 1-2 cell divisions over the 24-hour period to give rise to multiple daughter cells, at least one of which became associated with the neighboring ISV. We categorized sclerotome progenitors into three groups based on the final positions of perivascular fibroblasts they generated: 1) only at the dorsal ISV, 2) only at the ventral ISV, or 3) at both dorsal and ventral ISV (Fig. 2C). Sclerotome progenitors in the dorsal domain gave rise to exclusively perivascular fibroblasts along dorsal ISVs (20/20 cells, 100%) (Fig. 2C). Similarly, the majority of sclerotome progenitors around the notochord (i.e., sclerotome derived notochord associated cells) (21/23 cells, 91%) contributed to only perivascular fibroblasts at the dorsal ISV (Fig. 2C). By contrast, 48% of sclerotome progenitors in the ventral domain (38/79 cells) gave rise to only perivascular fibroblasts at the ventral ISV, 35% of ventral sclerotome progenitors (28/79 cells) generated only dorsal perivascular fibroblasts, while the remaining 16% of ventral progenitors (13/79 cells) contributed to perivascular fibroblasts at both dorsal and ventral ISV regions (Fig. 2C). Similar to the contribution of tendon fibroblasts (tenocytes) (46), the dorsal sclerotome generates only dorsally positioned perivascular fibroblasts, whereas the ventral sclerotome contributes to perivascular fibroblasts along the entire D-V axis of ISVs (the combined bar in Fig. 2C). Moreover, perivascular fibroblasts along a given ISV were always derived from the sclerotome of the same overlying somite (170/170 cells, 100%). Together, our results demonstrate that perivascular fibroblasts originate from all three sclerotome compartments in a stereotypic manner.

Perivascular fibroblasts are distinct from pericytes

Mural cells, including pericytes and vSMCs, are known blood vessel associated support cells. We next asked whether perivascular fibroblasts represent a different perivascular cell population from mural cells. In the zebrafish trunk, pericytes are associated with ISVs, while vSMCs are localized to larger vessels such as the dorsal aorta (43,45). Platelet derived growth factor (PDGF) signaling is

known to play an important role in pericyte recruitment and the platelet derived growth factor receptor-beta (*pdgfrb)* is a well-established pericyte marker (45; 47-48). We utilized the *pdgfrb:Gal4FF; UAS:NTR-mCherry* line (referred to as *pdgfrb*$^{NTR\text{-}mCherry}$) to label pericytes, while the *nkx3.1*$^{NTR\text{-}mCherry}$ and *col1a2:GFP* reporters were used to mark perivascular fibroblasts. Our results indicate that perivascular fibroblasts and pericytes represent distinct cell populations. First, they showed different developmental timing and cell numbers. Consistent with our time-lapse movies, *nkx3.1*$^{NTR\text{-}mCherry}$-positive perivascular fibroblasts emerged along ISVs prior to 2 dpf (days post fertilization) (Fig. 1A and S2) and remained largely constant in number (9.9-10.7 per ISV) from 2 to 4 dpf (Fig. 3A). By contrast, pericytes marked by *pdgfrb*$^{NTR\text{-}mCherry}$ did not appear on ISVs until 3 dpf, and the cell number increased to 0.9 per ISV by 4 dpf (Fig. 3A), similar to what has been previously described (45). Second, perivascular fibroblasts and pericytes showed distinct marker expression (Fig. 3B). Perivascular fibroblasts labeled by *col1a2:GFP* did not express the *pdgfrb*$^{NTR\text{-}mCherry}$ reporter at 4 dpf. Conversely, *pdgfrb*$^{NTR\text{-}mCherry}$-positive pericytes showed minimal *col1a2:GFP* expression. While perivascular fibroblasts appeared globular, pericytes were more elongated with long cellular processes (Fig. 3B). Moreover, perivascular fibroblasts were more laterally located along ISVs compared to pericytes, with pericyte processes often sandwiched between the neighboring perivascular fibroblasts and the endothelium (Fig. 3B). To further examine the morphological differences between perivascular fibroblasts and pericytes, we performed high resolution confocal microscopy at the single cell resolution at 3 dpf. *pdgfrb*$^{NTR\text{-}mCherry}$-positive pericytes showed the typical pericyte morphology: small and flat cell bodies with several elongated cellular processes that extended longitudinally along and tightly wrapped around the ISV, labeled by *kdrl:EGFP* (Fig. 3C). Since perivascular fibroblasts are more abundant along ISVs compared to pericytes, we took advantage of a mosaic *col1a2:Gal4; UAS:Kaede* line (referred to as *col1a2*^{Kaede}) (49) to sparsely label single perivascular fibroblasts for easier visualization. In contrast to pericytes, perivascular fibroblasts were more loosely associated with ISVs and had a globular morphology with shorter and finer processes that wrapped diametrically around the associated ISV in an ‘awkward hug’ (Fig. 3D). Taken together, our results suggest that perivascular fibroblasts and pericytes represent two distinct populations of perivascular cells with unique marker expression, morphology, distribution and developmental timing.

A sub-population of perivascular fibroblasts functions as pericyte progenitors

While occupying the similar perivascular space, perivascular fibroblasts appear along ISVs at least one day before pericytes (Fig. 3A). We hypothesized that perivascular fibroblasts act as progenitors for ISV pericytes. To test this possibility, we conducted time-lapse imaging of *pdgfrb*$^{NTR\text{-}mCherry}$*; col1a2:GFP* embryos from 54 to 73 hpf during which pericytes started to appear on ISVs.

Interestingly, a subset of *col1a2:GFP*-positive perivascular fibroblasts gradually lost GFP expression, switched on the pericyte reporter *pdgfrb*$^{NTR\text{-}mCherry}$, and developed long cellular processes characteristic of pericytes at this stage (Fig. 4A and Movie S2). Indeed, of 15 newly formed pericytes traced in our time-lapse movies, 60% were derived from *col1a2:GFP*-expressing perivascular fibroblasts (9/15 cells). This result suggests that a sub-population of perivascular fibroblasts can differentiate into pericytes. Since *col1a2* transgenic lines such as *col1a2:GFP* are mosaic (Fig. S3A) (49), the number above likely under-estimates the proportion of pericytes derived from perivascular fibroblasts. To further test our model, we performed time-lapse experiments in *nkx3.1*$^{NTR\text{-}mCherry}$*; pdgfrb:GFP* embryos. Interestingly, while both *pdgfrb:GFP* and *pdgfrb*$^{NTR\text{-}mCherry}$ lines labeled pericytes (GFP^{high}mCherry^{+} expression) at 4 dpf, *pdgfrb:GFP* but not *pdgfrb*$^{NTR\text{-}mCherry}$ also marked perivascular fibroblasts (GFP^{low}mCherry^{-} expression) at 2 and 4 dpf (Fig. S3B and S3C). This is consistent with the previous report that the sclerotome expresses *pdgfrb* (50), suggesting that *pdgfrb:GFP* is a more sensitive reporter than the *pdgfrb*$^{NTR\text{-}mCherry}$ line. Similar to movies in *pdgfrb*$^{NTR\text{-}mCherry}$*; col1a2:GFP* embryos, cell tracing in *nkx3.1*$^{NTR\text{-}mCherry}$*; pdgfrb:GFP* embryos showed that some mCherry^{+}GFP^{low} perivascular fibroblasts slowly upregulated GFP expression, and extended pericyte-like cellular processes wrapping around the ISV (Movie S3). Of 117 newly formed GFP^{high} pericytes, 91% of them (106/117 cells) were derived from mCherry^{+} perivascular fibroblasts. This result confirms that a sub-population of perivascular fibroblasts functions as pericyte precursors. Since perivascular fibroblasts originate from the sclerotome, we conclude that most pericytes along ISVs are also derived from the sclerotome.

To further test if perivascular fibroblasts serve as pericyte precursors, we performed genetic ablation of perivascular fibroblasts using the *col1a2:Gal4; UAS:NTR-mCherry* line (referred to as *col1a2*$^{NTR\text{-}mCherry}$). Nitroreductase (NTR) converts metronidazole (MTZ), an otherwise harmless prodrug into a cytotoxic compound, resulting in the death of NTR-expressing cells (51). To ablate perivascular fibroblasts prior to pericyte differentiation, *col1a2*$^{NTR\text{-}mCherry}$*; pdgfrb:GFP* embryos were treated with MTZ from 1 to 3 dpf, after which the drug was washed off and embryos were imaged for pericytes at 4 dpf (Fig. 4B). In contrast to water-treated controls, we observed a complete loss of perivascular fibroblasts in MTZ-treated embryos, with only residual mCherry^{+} debris visible in the trunk (Fig. 4C). Interestingly, we observed a drastic 3.5-fold reduction in the number of pericytes in MTZ-treated embryos (0.4 cells per ISV) compared to water-treated controls (1.4 cells per ISV) (Fig. 4C and 4D). This result is consistent with our model that perivascular fibroblasts function as pericyte precursors as depletion of perivascular fibroblasts leads to the decrease in the number of pericytes. Together, our work suggests that the sclerotome generates perivascular fibroblasts, some of which further differentiate into pericytes along the ISVs.

246

247 **Loss of perivascular fibroblasts results in dysmorphic ISVs**

248 Our work suggests that perivascular fibroblasts function as progenitors to generate pericytes to
249 support the vasculature. However, only a small fraction of perivascular fibroblasts actually
250 differentiates into pericytes, raising the question about the function of the remaining perivascular
251 fibroblasts. Moreover, the emergence of perivascular fibroblasts occurs concurrently with ISV
252 development (Fig. 2B and S2; Movie S1), well before pericyte differentiation at 60 hpf (45). These
253 observations raise the possibility that perivascular fibroblasts play an early role in stabilizing nascent
254 blood vessels prior to pericyte formation. To test this idea, we examined the impact of early ablation of
255 perivascular fibroblasts on ISV development using the nitroreductase-based system. *nkx3.1*$^{NTR\text{-}mCherry}$*;*
256 *kdrl:EGFP* embryos were incubated in water or MTZ for a 24 hour period starting at 38 hpf when ISV
257 formation was complete and blood flow had commenced in ISVs (Fig. 5A). ISV morphology was
258 examined after the drug treatment at 62 hpf. Water-treated control embryos showed stereotypical
259 ISVs with many mCherry^{+} perivascular fibroblasts (Fig. 5B). MTZ treatment resulted in a complete
260 loss of perivascular fibroblasts, with only some mCherry^{+} cell debris remaining (Fig. 5B). Compared to
261 control ISVs, most ISVs in ablated embryos showed visible distortions in their diameters, shrinking
262 and dilating dramatically at different points along the ISV length (Fig. 5B). To quantify this variability,
263 the diameter of each ISV was measured at four equidistant points along its length and standard
264 deviation from the mean diameter was graphed as a readout for ISV diameter variability (Fig. 5C).
265 Indeed, ISVs in the absence of perivascular fibroblasts were significantly more variable than those of
266 water-treated controls (Fig. 5C). Interestingly, similar ablation experiments using *col1a2*$^{NTR\text{-}mCherry}$*;*
267 *kdrl:EGFP* during later stages between 4 and 5 dpf did not significantly alter the ISV morphology (Fig.
268 S4). Together, our results suggest that perivascular fibroblasts play an early role in the stabilization of
269 nascent blood vessels but are dispensable for maintaining ISV morphology at later stages.

270

271 **Perivascular fibroblasts deposit collagens around ISVs**

272 Our work suggests that perivascular fibroblasts are crucial for the stabilization of nascent ISVs.
273 Since perivascular fibroblasts show high-level expression of collagen genes, including *col1a2* and
274 *col5a1,* we predicted that perivascular fibroblasts are the main source of the vascular ECM around
275 newly formed ISVs. To test this model, we generated a *UAS:Col1a2-GFP* construct to express GFP-
276 fused Col1a2 in live embryos. A similar *Col1a2-GFP* reporter has been previously used to visualize
277 collagen deposition during skin development and repair in zebrafish (52). *nkx3.1:Gal4; UAS:NTR-*
278 *mCherry* embryos injected with the *UAS:Col1a2-GFP* plasmid showed many mCherry^{+}GFP^{+}
279 perivascular fibroblasts surrounding ISVs at 56 hpf (Fig. 5D). Indeed, numerous thin GFP^{+} 'strings',

likely corresponding to collagen fibers, wrapped around the ISV with the intensity increasing from 56 to 72 hpf, suggesting continuous Col1a2-GFP protein deposition (Fig. 5D). To determine whether perivascular fibroblasts directly contribute to collagens around ISVs, we injected *nkx3.1*$^{NTR\text{-}mCherry}$ embryos with a low dose of the *UAS:Col1a2-GFP* plasmid to achieve mosaic labeling of perivascular fibroblasts. Imaging of individually labeled mCherry^{+}GFP^{+} perivascular fibroblasts showed local Col1a2-GFP deposition around the ISV within 1-2 cell diameters from the Col1a2-GFP-expressing perivascular fibroblast (Fig. 5E). Our results suggest that perivascular fibroblasts contribute to collagens in the ECM surrounding nascent ISVs that likely contribute to vessel stabilization.

collagen mutants display severe ISV hemorrhage

Our work suggests that perivascular fibroblasts secrete collagens and stabilize nascent ISVs. We next asked whether Col1a2 and Col5a1, which are expressed in perivascular fibroblasts (Fig. 1C and S1), are required to maintain the integrity of nascent blood vessels. Using CRISPR/Cas9 editing (53), we generated mutants for *col1a2* (*col1a2*^{ca108}, 1-bp deletion) and *col5a1* (*col5a1*^{ca109}, 4-bp deletion) (Fig. S5A and S5B). Both alleles resulted in frame shifts in the corresponding coding sequences leading to premature stops (Fig. S5C and S5D). For simplicity, we designate wild-type, heterozygous or homozygous fish as *+/+*, *+/-*, and *-/-*, respectively. For example, heterozygous carriers of *col1a2*^{ca108} are referred to as *col1a2*$^{+/-}$. Whole mount in situ hybridization showed that mutant mRNAs for both genes underwent nonsense-mediated decay (Fig. 6A), suggesting that both *col1a2*^{ca108} and *col5a1*^{ca109} are null alleles. Crosses of heterozygous *col1a2*$^{+/-}$ parents gave rise to progeny segregated in roughly Mendelian ratios at all stages examined (Fig. S6A). Although homozygous *col1a2*$^{-/-}$ mutants were viable as adults, they were substantially smaller than their wild-type siblings and often showed severe spine curvature (Fig. S6B). This phenotype is reminiscent of those described in other type I collagen mutants (54,55). By contrast, from crosses of heterozygous *col5a1*$^{+/-}$ parents, homozygous *col5a1*$^{-/-}$ mutants were under-represented at 11 dpf, and completely absent by 14 dpf (Fig. S6C). These results suggest that Col5a1 is a more critical component of the ECM compared to Col1a2, and it is required for the survival of the fish to adulthood. Strikingly, a small percentage of homozygous *col5a1*$^{-/-}$ embryos showed spontaneous hemorrhage in the trunk region at 2 dpf, suggesting compromised vascular integrity in the absence of Col5a1 (Fig. 6B).

To further characterize the hemorrhage phenotype in *collagen* mutants, we developed a phenotype screening procedure (Fig. 6C). In this assay, we analyzed both single mutants as well as double mutants to test genetic interactions between *col1a2* and *col5a1*. In addition, we tested whether the increase in physical stress exacerbates the hemorrhage phenotype by raising embryos in a high-viscosity medium (0.6% methylcellulose, MC) (56). Briefly, heterozygous adults harboring either one

or both of the *collagen* mutations (*col1a2*$^{+/-}$, *col5a1*$^{+/-}$, or *col1a2*$^{+/-}$; *col5a1*$^{+/-}$) were intercrossed to generate wild type, heterozygous, and homozygous sibling embryos for different combinations (Fig. 6C). The resulting embryos were then incubated in either water or the viscous methylcellulose solution from 48 to 80 hpf, during which embryos were imaged and screened for hemorrhage in the trunk. Embryos were then genotyped to correlate the genotype with the phenotype. Similar to their wild-type *col1a2*$^{+/+}$ siblings (water: 0/14; MC: 0/27) and heterozygous *col1a2*$^{+/-}$ siblings (water: 0/39; MC: 0/38), homozygous *col1a2*$^{-/-}$ mutants did not show any trunk hemorrhage in either water (0/22) or the methylcellulose solution (0/21). This result suggests that loss of *col1a2* alone does not compromise vascular stability even with increased physical stress. By contrast, while neither wild-type *col5a1*$^{+/+}$ embryos (0/11) nor heterozygous *col5a1*$^{+/-}$ siblings (0/39) showed any hemorrhage under normal conditions, 12% of *col5a1*$^{-/-}$ embryos (3/25) displayed obvious hemorrhages in the trunk at 2 dpf, which was worsened substantially by physical stress (17/26, 65%). Analysis of different allele combinations of double mutants revealed several key characteristics of the hemorrhage phenotype (Fig. 6D). First, the loss of both *col5a1* wild-type alleles was required to cause the trunk hemorrhage phenotype. Second, even though loss of *col1a2* alone in *col1a2*$^{+/-}$ or *col1a2*$^{-/-}$ embryos was not sufficient to cause hemorrhage, loss of one or two *col1a2* wild-type alleles progressively increased the penetrance of the hemorrhage phenotype in *col5a1*$^{-/-}$ mutants, from 23% in *col1a2*$^{+/-}$; *col5a1*$^{-/-}$ embryos (5/22) to 58% in *col1a2*$^{-/-}$; *col5a1*$^{-/-}$ embryos (7/12) (Fig. 6D). Lastly, increased physical stress by incubating embryos in the viscous methylcellulose solution substantially exacerbated both the penetrance and the severity of the hemorrhage phenotype (Fig. 6D, 6E and S6D). It is interesting to note that stress-induced blood vessel rupture is typical of the vascular phenotypes associated with classical Ehlers-Danlos syndrome in humans. Together, our mutant analysis suggests that Col5a1 and Col1a2 function redundantly to maintain blood vessel integrity with Col5a1 being a more critical component.

The distribution of hemorrhagic foci is consistent with defects in ISVs in the trunk. To directly examine the ISV morphology in *collagen* mutants, we crossed *col5a1*$^{+/-}$*; kdrl:EGFP* adults with *col1a2*$^{+/-}$*; col5a1*$^{+/-}$ double heterozygous fish. Resulting embryos were incubated in the methylcellulose solution and their ISVs were analyzed at 53 hpf. In contrast to wild-type siblings, some *col5a1*$^{-/-}$ mutants showed severe ISV deformity and breakage, accompanied by hemorrhage (Fig. 6F). Quantifications of the diameter variability of intact ISVs as described earlier showed that both *col1a2*$^{+/+}$; *col5a1*$^{-/-}$ and *col1a2*$^{+/-}$; *col5a1*$^{-/-}$ embryos displayed significantly more variable ISVs than wild-type siblings (Fig. 6G). Consistent with a stronger hemorrhage phenotype, ISVs in *col1a2*$^{+/-}$; *col5a1*$^{-/-}$ embryos were significantly more variable than those in *col1a2*$^{+/+}$; *col5a1*$^{-/-}$ single mutants.

347 Together, our work suggests that the deposition of Col5a1 and Col1a2 between 1-2 dpf, likely by
348 perivascular fibroblasts, is crucial for the stabilization of nascent ISVs.

DISCUSSION

In this study, we characterize the origin and function of perivascular fibroblasts, a novel population of blood vessel associated cells in zebrafish. Our work provides three main conclusions. First, perivascular fibroblasts originate from the sclerotome and are distinct from pericytes. Second, a subset of perivascular fibroblasts functions as pericyte progenitors. Third, cell ablation and mutant analysis reveal that perivascular fibroblasts stabilize nascent blood vessels through Col1a2 and Col5a1. Together, we propose a dual role of perivascular fibroblasts in vascular stabilization: they first establish the ECM around nascent blood vessels for initial stabilization and then function as pericyte progenitors to generate pericytes that further contribute to vessel integrity (Fig. 7). Our work provides new insights into the molecular and cellular mechanisms underlying vascular stabilization and vascular diseases, such as Ehlers-Danlos syndrome.

Perivascular fibroblasts are a unique population of perivascular cells

Mural cells are well studied blood vessel support cells. In the zebrafish trunk, each intersegmental vessel is associated with 1-2 pericytes at 4 dpf. Four lines of evidence suggest that collagen-expressing perivascular fibroblasts represent a unique population of perivascular cells, distinct from pericytes. First, these two cell populations show distinct marker expression, with pericytes labeled by *pdgfrb,* and perivascular fibroblasts marked by the expression of collagen genes, such as *col1a2* and *col5a1*. Second, perivascular fibroblasts become associated with ISVs as early as 31 hpf, whereas pericytes do not differentiate until at least 60 hpf (45). Third, perivascular fibroblasts are much more abundant than pericytes, with on average 10.6 perivascular fibroblasts per ISV compared to 0.9 pericytes per vessel at 4 dpf. Finally, perivascular fibroblasts and pericytes display vastly distinct morphologies. Similar to mammalian pericytes, ISV pericytes in zebrafish have small and flat cell bodies with long cellular processes that tightly wrap around and along the underlying endothelium. By contrast, perivascular fibroblasts are more loosely associated with ISVs, and appear more globular with numerous shorter and thinner processes that extend around the endothelium. Based on the differences in marker expression, developmental timing, cell number, and cell morphology, we propose that perivascular fibroblasts represent a novel perivascular cell population, distinct from pericytes. Intriguingly, recent single cell RNA sequencing studies have revealed a similar perivascular 'fibroblast-like' cell population in the adult murine brain (Saunders et al., 2018; Vanlandewijck et al., 2018). Similar to zebrafish perivascular fibroblasts, murine fibroblast-like cells are loosely adhered to the blood vessels, abluminal to mural cells and the basement membrane. Furthermore, murine fibroblast-like cells robustly express many ECM genes, including collagen genes *col5a1* and *col1a2,*

but not mural cell markers such as *pdgfrb*. Combined with our work, these studies suggest that perivascular fibroblasts represent a unique and evolutionarily conserved population of blood vessel associated cells across vertebrates.

The sclerotome is the embryonic origin of perivascular fibroblasts

The sclerotome is the embryonic compartment that contributes to the axial skeleton of vertebrates. Our previous and current studies demonstrate that the sclerotome also gives rise to several populations of tissue support cells, including tenocytes (tendon fibroblasts) (46) and perivascular fibroblasts. The zebrafish sclerotome has a unique bipartite organization with a larger ventral domain and a smaller dorsal domain. Using time-lapse imaging and cell tracing, we have built a spatial map of origin for perivascular fibroblasts. Similar to tenocytes, the ventral sclerotome domain is the main contributor of perivascular fibroblasts (84%). Furthermore, different sclerotome domains contribute to perivascular fibroblasts with a stereotypic spatial pattern. The ventral sclerotome domain generates perivascular fibroblasts along the entire length of the ISV, whereas the dorsal sclerotome domain contributes only locally to perivascular fibroblasts associated with the dorsal half of the ISV. Since perivascular fibroblasts also function as pericyte precursors (see below), our results suggest that most pericytes associated with ISVs also originate from the sclerotome. Consistent with our results, vSMCs around the dorsal aorta have been traced back to cells derived from the sclerotome in zebrafish (50). In addition, mural cells in the zebrafish trunk vessels have been shown to be dependent on the mesoderm but not the neural crest lineage (57). Thus, blood vessel support cells in the zebrafish trunk, including perivascular fibroblasts and mural cells, likely originate from the sclerotome. Combined with previous lineage analysis in mouse and chick (58, 59), these data suggest a model where mural cells in the brain are neural crest derived, whereas mural cells in the trunk are sclerotome derived.

Perivascular fibroblasts function as pericyte progenitors

Although perivascular fibroblast-like cells have been identified in the mouse brain by single cell RNA sequencing, their biological functions are still unclear. Two complementary experiments suggest that perivascular fibroblasts function as pericyte progenitors. First, in vivo imaging reveals that the majority of newly born pericytes on ISVs at 3 dpf can be traced back to perivascular fibroblasts at 2 dpf. Indeed, time-lapse imaging in both *nkx3.1*$^{NTR\text{-}mCherry}$*; pdgfrb:GFP* and *col1a2:GFP; pdgfrb*$^{NTR\text{-}mCherry}$ embryos reveals similar kinetics of pericyte differentiation: a few perivascular fibroblasts gradually downregulate their fibroblast marker expression, upregulate pericyte reporters, and undergo morphological changes to extend long pericyte-like processes along ISVs at 3 dpf. In complementary

experiments, genetic ablation of perivascular fibroblasts results in a 3.5-fold reduction in the number of pericytes. Together, these results indicate that some perivascular fibroblasts serve as pericyte precursors, contributing to most, if not all, pericytes associated with ISVs in the trunk. Incomplete labeling or ablation likely reflects the mosaic nature of the *col1a2* transgenic lines (49).

It is interesting to note that there are about 10 perivascular fibroblasts associated with each ISV, however, only 1-2 of these cells differentiate into pericytes. It thus raises the question of how these perivascular fibroblasts are 'selected' as pericyte progenitors. There are two possibilities. In the first scenario, all perivascular fibroblasts have the equal potential to differentiate into pericytes, but extrinsic cues determine which cell to switch on the pericyte fate. Notch signaling has been implicated in the regulation of pericyte formation in both mouse and zebrafish (57; 60-63). In particular, recent work in zebrafish has shown that the activation of Notch signaling in naïve mesenchymal cells (likely corresponding to perivascular fibroblasts in our study) is crucial to induce pericyte differentiation around ISVs (Ando et al., 2019). Therefore, active Notch signaling might bias some perivascular fibroblasts towards the pericyte lineage. Alternatively, perivascular fibroblasts might represent a heterogenous population of cells, containing a small fraction of pericyte progenitors. Supporting this idea, recent scRNA sequencing studies have shown that perivascular fibroblast-like cells in the mouse brain can be further divided into several subtypes based on unique gene expression signatures (Saunders et al., 2018; Vanlandewijck et al., 2018).

Perivascular fibroblasts function to stabilize nascent blood vessels

Although mural cells are known to stabilize mature blood vessels, it is not clear how newly formed blood vessels are supported prior to the differentiation of mural cells. Our work provides strong evidence that perivascular fibroblasts function to stabilize nascent blood vessels by secreting collagens. First, time-lapse imaging reveals that the emergence of perivascular fibroblasts along ISVs occurs concurrently with ISV development, at least one day before the differentiation of the first pericytes. Second, genetic ablation of perivascular fibroblasts prior to pericyte differentiation results in aberrant ISV morphology. By contrast, late ablation of perivascular fibroblasts from 4 to 5 dpf has no effects on the ISV morphology. These results suggest that perivascular fibroblasts play a crucial role in supporting newly formed blood vessels before pericyte differentiation. Lastly, perivascular fibroblasts express high level of collagen genes, such as *col1a2* and *col5a1*, and contribute to the vascular collagen surrounding ISVs. The live Col1a2-GFP reporter reveals that perivascular fibroblasts contribute to a network of collagen fibers around nascent ISVs as early as 2 dpf, which continues to expand until at least 3 dpf. Strikingly, loss of *col5a1* results in dysmorphic ISVs with spontaneous hemorrhage in the trunk, which is exacerbated by the additional loss of *col1a2* or

increasing physical stress. It is important to note that these ISV phenotypes can be observed as early as 2 dpf, well before the emergence of pericytes on ISVs. Together, our experiments show that perivascular fibroblasts act to stabilize nascent ISVs prior to pericyte differentiation, likely through regulating collagen deposition. Interestingly, ablation of perivascular fibroblasts rarely results in the severe hemorrhage phenotype observed in *col5a1*$^{-/-}$ mutants (under either normal or stressed conditions). One possible explanation is that the few perivascular fibroblasts spared from the ablation due to transgene mosaicism might be sufficient to prevent ISV rupture. Consistent with our work, recent study has described a similar population of *col22a1*$^{+}$ perivascular fibroblast-like cells associated with the cranial vasculature in zebrafish (64). Null mutations in c*ol22a1,* a minor fibril-associated collagen, result in compromised cranial vessel integrity in both embryos and adults following cardiovascular stress (64), highlighting the importance of collagen and perivascular fibroblasts in vascular stabilization.

Zebrafish model of Ehlers-Danlos syndrome

Collagen is the most abundant protein in the human body and is a major component of the ECM (65). Fibrillar collagens, including collagen I and collagen V, constitute the most common sub-group within the collagen family which often co-localize in tissues such as the dermis, tendons and ligaments (65). Mutations in fibrillar collagens or collagen modification enzymes have been implicated in a number of connective tissue diseases, including Ehlers-Danlos syndrome (EDS). The classical subtype of EDS, caused by mutations in collagen V, and less frequently collagen I, is characterized by skin hyperextensibility, joint hypermobility, and blood vessel fragility (19,66). Classical EDS patients experience easy bruising and excessive hemorrhaging under normal exertion. By contrast, vascular phenotypes are more prominent in the vascular subtype of EDS, resulting from mutations in collagen III, with most patients experiencing severe spontaneous rupture of large arteries (19). Interestingly, the zebrafish genome does not contain a collagen III gene, which is likely lost during evolution as in many other teleost fish species (67). Characterization of zebrafish *col1a2* and *col5a1* mutants reveals several key features of vascular EDS. Embryos lacking functional *col5a1* genes develop spontaneous hemorrhages in the trunk under normal physiological conditions, reminiscent of easy bruising in patients with vascular EDS. One hallmark of vascular EDS is that physical stress often leads to more severe symptoms (68). Similarly, both the penetrance and severity of the hemorrhage phenotype in *col5a1*$^{-/-}$ mutants are strongly enhanced by the increase of physical stress. Thus, our results suggest that the lack of collagen III in zebrafish is likely compensated by other fibrillar collagens (types I and V). Our *col1a2* and *col5a1* mutants represent the first zebrafish model of vascular EDS that we know of.

Analysis of collagen mutants also provides new insights on vascular EDS. First, Col5a1 is a more critical component of the vascular ECM compared to Col1a2. Lack of *col5a1* function leads to ISV hemorrhages, whereas loss of *col1a2* alone does not result in any obvious vascular defects even with increased physical stress. Intriguingly, collagen I is the most abundant component in collagen fibrils (> 90%), while collagen V constitutes only a minor fraction (< 5%) (69). Why do *col5a1*$^{-/-}$ mutants show more severe phenotypes than *col1a2*$^{-/-}$ mutants? Previous work has shown that Col5a1 plays an important role in proper nucleation and diameter regulation of collagen fibrils (70). The loss of Col5a1 might result in defects in the assembly of collagen I into fibrils, leading to a more severe phenotype. Second, our mutant analysis reveals genetic interactions between *col1a2* and *col5a1*. Loss of wild-type *col1a2* alleles in the *col5a1*$^{-/-}$ background substantially enhances both the penetrance and the severity of the hemorrhage phenotype in a dosage dependent manner. This result suggests that Col5a1 and Col1a2 function redundantly to maintain vascular integrity. Lastly, as discussed above, our work provides strong evidence that defects in perivascular fibroblasts are the underlying cellular basis for the vascular phenotypes of EDS patients. Perivascular fibroblasts thus represent the cellular targets for potential therapeutic interventions.

In summary, our work identifies perivascular fibroblasts as a novel perivascular cell population with dual function in vascular stabilization: they regulate the ECM of nascent blood vessels and also function as pericyte progenitors. Interestingly, many perivascular fibroblasts remain associated with mature blood vessels even after pericyte differentiation. This raises several questions about the function of these cells at later stages. Do perivascular fibroblasts continue to regulate the ECM around the mature vasculature? Do they function as resident stem cells to replace aging/damaged pericytes? Previous work has suggested that tissue injury in the mouse brain and spinal cord often triggers a fibrotic response by blood vessel associated cells (25,34–36). Attenuation of the fibrotic response has been shown to limit scar formation and improve axon regeneration post spinal cord injury in mice, suggesting that perivascular stromal cells might be an important therapeutic target (71). It is plausible that zebrafish perivascular fibroblasts also play an active role in tissue injury repair, an exciting question for future investigations.

MATERIALS AND METHODS

Zebrafish strains

Zebrafish strains were maintained according to standard protocols. Animal research was conducted in accordance with current guidelines of the Canadian Council on Animal Care. All protocols were approved by the Animal Care Committee at the University of Calgary (#AC17-0128). The following transgenic strains were utilized in this study: *TgBAC(col1a2:Gal4)ca102* (46, 49), *TgBAC(col1a2:GFP)ca103* (46), *Tg(kdrl:EGFP)la116* (72), *Tg(kdrl:mCherry)ci5* (73), *TgBAC(nkx3.1:Gal4)ca101* (46), *TgBAC(pdgfrb:Gal4FF)ca42* (45,74), *TgBAC(pdgfrb:GFP)ca41* (45), *Tg(UAS:Kaede)s1999t* (75), *Tg(UAS:NTR-mCherry)c264* (75). The mosaic *col1a2:Gal4; UAS:Kaede* line was maintained by growing embryos with more mosaic Kaede expression. The *col1a2*^{ca108} and *col5a1*^{ca109} mutant lines were maintained as heterozygotes, and homozygous embryos were generated by intercrossing heterozygous carriers.

Generation of CRISPR mutants

The *col1a2*^{ca108} and *col5a1*^{ca109} mutant lines were generated using the CRISPR/Cas9 system as previously described (53). Briefly, target sites were identified using the web program CHOPCHOP (http://chopchop.cbu.uib.no) (76). sgRNA target sequences are 5'-GGGGGTTCCATTTGATCCAG-3' (*col1a2*) and 5'-GGCTCCAGCAGATCATCCAG-3' (*col5a1*). To assemble DNA templates for sgRNA transcription, gene-specific oligonucleotides containing the T7 promoter sequence (5'-TAATACGACTCACTATA-3'), the 20 base target site, and a complementary sequence were annealed to a constant oligonucleotide encoding the reverse-complement of the tracrRNA tail. sgRNAs were generated by in vitro transcription using the Megascript kit (Ambion). Cas9 mRNA was transcribed from linearized pCS2-Cas9 plasmid using the mMachine SP6 kit (Ambion). To generate mutants, one-cell stage wild-type embryos were injected with a mix containing the appropriate sgRNA at 20 ng/μl and Cas9 mRNA at 200 ng/μl. Injected fish were raised to adulthood and crossed to generate F1 embryos. T7 Endonuclease I assay (NEB) was then used to identify the presence of indel mutations in the targeted region of F1 fish. A *col1a2* allele containing 1 bp deletion (*col1a2*^{ca108}) and a *col5a1* allele with 4 bp deletion (*col5a1*^{ca109}) were identified (Fig. S5). For genotyping, small regions around the mutation sites were specifically amplified by PCR, which was followed by allele-specific restriction enzyme analysis. For *col1a2*^{ca108}, the primers used were 5'-TTTTAAAGACTCACATTTGCCTT-3' (forward) and 5'-CTCCGGGCTAGCTTTATATTTCGATT-3' (reverse). For *col5a1*^{ca109}, the primers used were 5'-ACTCTTGTTTGCTGTGCAGGT-3' (forward) and 5'-CTCACCGGTATTGGCCGTGTT-3' (reverse). Following PCR, the products were digested with a restriction enzyme which cuts only the

wild type or the mutant allele. The enzymes used were BclI and BstCI (NEB) for *col1a2*^{ca108} and *col5a1*^{ca109}, respectively. The resulting band sizes were analyzed using gel electrophoresis. For *col1a2*^{ca108}, the BclI digest resulted in a single band of 473 bp in wild-type embryos, and two bands of 400 bp and 73 bp in homozygous *col1a2*$^{-/-}$ embryos. For *col5a1*^{ca109}, the BstCI digest resulted in multiple bands at 89, 44, 30, 18 and 9 bp in wild-type embryos, and bands of 107, 44, 30 and 9 bp in homozygous *col5a1*$^{-/-}$ embryos.

Plasmid injection

To visualize collagen distribution, we generated a *UAS:Col1a2-GFP* construct based on a previously published *pME-Col1a2-GFP* plasmid (52). *UAS:Col1a2-GFP* (40 ng/μl) was co-injected with *tol2* transposase mRNA (40 ng/μl) into *nkx3.1:Gal4; UAS:NTR-mCherry* embryos at the one-cell stage with 1 nl per embryo. For more mosaic labeling, *UAS:Col1a2-GFP* was injected at 10 ng/μl. Injected embryos were screened for GFP expression at appropriate stages for imaging.

In situ hybridization and immunohistochemistry

Whole-mount in situ hybridization and antibody staining were performed according to standard protocols. *col1a2* and *col5a1* antisense probes were used in this study. Double fluorescent in situ hybridization was performed using digoxigenin (DIG) and dinitrophenyl (DNP) labeled probes. For antibody labeling, the rabbit polyclonal antibody to GFP (1:500, MBL) was used. For fluorescent detection of antibody labeling, appropriate Alexa Fluor-conjugated secondary antibodies were used (1:500, Thermo Fisher).

Time-lapse imaging

Imaging was performed using the Olympus FV1200 confocal microscope as previously described (46). Embryos older than 24 hpf were incubated in fish water with 1-phenyl 2-thiourea (PTU) to prevent pigmentation. Fish were anesthetized in 0.4% tricaine and mounted in 0.6% low melting point agarose. Z-stack images of the region of interest were then collected using the 20x objective at appropriate time intervals (5-15 mins) for up to 24 hours. Movies and images were processed using the Olympus Fluoview software and the Fiji software (77). Cell tracing was performed manually using Fiji.

Cell ablation

To ablate perivascular fibroblasts, *nkx3.1*$^{NTR\text{-}mCherry}$ or *col1a2*$^{NTR\text{-}mCherry}$ embryos at desired developmental stages were treated with water (control group) or 5 mM metronidazole (MTZ,

581 experimental group) for 24-48 hours. In some experiments, mCherry^{-} siblings treated with 5 mM MTZ
582 in the same time windows were used as additional controls. Embryos were subsequently washed in
583 fish water and imaged to confirm successful ablation of mCherry^{+} cells.
584
585 **Quantification of blood vessel diameter variability**
586 To quantify blood vessel diameters, we used the endothelial specific *kdrl:GFP* reporter to
587 fluorescently label intersegmental vessels. Embryos were imaged laterally in the trunk region (somite
588 12 to 18) and 8-10 ISVs were quantified per embryo. Using the 'line selection' tool in Fiji, four
589 diameter measurements were taken for each ISV at equidistant points along its length and
590 measurements were averaged to obtain mean vessel diameter. Standard deviation from the mean
591 vessel diameter was plotted as a readout of ISV diameter variability.
592
593 **Mechanical stress assay**
594 To test the effect of physical stress on the vascular phenotype of collagen mutants, we adopted a
595 mechanical overloading assay by raising embryos in a high-viscosity medium (0.6% methylcellulose)
596 (56). Heterozygotes for single mutants (*col1a2*$^{+/-}$ or *col5a1*$^{+/-}$) or double mutants (*col1a2*$^{+/-}$*; col5a1*$^{+/-}$)
597 were intercrossed to obtain sibling embryos with different allele combinations. Resulting embryos
598 were incubated in water (control group) or 0.6% methylcellulose (MC, experimental group) at 48 hpf.
599 Fish were screened for hemorrhage in the trunk region approximately every 3 hours from 48 to 80 hpf
600 and subsequently genotyped for *col1a2* and *col5a1.*
601
602 **Statistical analysis**
603 All graphs and statistical analysis were generated using the GraphPad PRISM software. Data
604 were plotted with mean ± SEM indicated. Significance was calculated by performing using the non-
605 parametric Mann-Whitney *U* test with two-tailed p values: $p > 0.05$ (ns, not significant), $p < 0.05$ (*), p
606 < 0.01 (**), $p < 0.001$ (***) and $p < 0.0001$ (****).

ACKNOWLEDGEMENTS

We thank the zebrafish community for providing probes and reagents; Paul Martin for sharing the *Col1a2-GFP* plasmid; Sarah Childs for sharing transgenic lines and providing critical input on this project; members of the Childs and Huang laboratories for discussions; and Paul Mains for critical comments on the manuscript.

COMPETING INTERESTS

The authors declare that no competing interests exist.

FUNDING

This study was supported by grants to P.H. from the Canadian Institute of Health Research (MOP-136926 and PJT-169113), Canada Foundation for Innovation John R. Evans Leaders Fund (Project 32920), and Startup Fund from the Alberta Children's Hospital Research Institute (ACHRI). A.M.R. was supported by the ACHRI Graduate Scholarship. D.J.Z. was supported by the Alberta Innovates Summer Research Studentship.

FIGURE LEGENDS

Fig. 1. Characterization of perivascular fibroblasts in zebrafish. (A) Lateral view of a three somite region in *nkx3.1*$^{NTR\text{-}mCherry}$*; kdrl:EGFP* embryos at 48 hpf. Many mCherry^{+} perivascular fibroblasts (red, arrowheads) were closely associated with intersegmental vessels (ISVs) labeled by endothelial marker *kdrl:EGFP* (green). *n* = 11 embryos. (B) Co-expression of *nkx3.1*$^{NTR\text{-}mCherry}$ and *col1a2:GFP* in perivascular fibroblasts (arrowheads) at 52 hpf. The ISV is indicated by dashed lines. *n* = 17 embryos. (C) Fluorescent mRNA in situ hybridization showing expression of fibrillar collagens *col1a2* (green, left) and *col5a1* (green, right) in perivascular fibroblasts (arrowheads) along ISVs marked by *kdrl:EGFP* (red) at 48 hpf. *n* = 15 embryos per staining. Scale bars: (A,C) 50 µm; (B) 25 µm.

Fig. 2. Generation of perivascular fibroblasts from different sclerotome domains. (A) Schematic representation of the bipartite organization of the zebrafish sclerotome and the generation of perivascular fibroblasts. At 24 hpf, the zebrafish sclerotome in each somite is divided into three compartments: the dorsal sclerotome, the ventral sclerotome, and sclerotome derived notochord associated cells. Note that notochord associated cells originate from the ventral sclerotome and are located about half-somite posterior to the corresponding somite. At 48 hpf, perivascular fibroblasts appear along the length of the intersegmental vessels (ISVs, green). The dotted line indicates the position of the horizontal myoseptum, which divides any given ISV into a dorsal half and a ventral half. Perivascular fibroblasts were quantified based on their final locations along each ISV: dorsal ISV (above the horizontal myoseptum) or ventral ISV (below the horizontal myoseptum). (B) Snapshots from time-lapse imaging of a *nkx3.1*$^{NTR\text{-}mCherry}$*; kdrl:EGFP* embryo from 25 hpf to 49.5 hpf. Perivascular fibroblasts along ISVs were retrospectively traced to determine their cell of origin. One cell from the ventral sclerotome domain (cyan arrows) and one cell from sclerotome derived notochord associated cells (yellow arrows) were traced over 24.5 hours with their daughter cells indicated by the same colored arrows/arrowheads. Both sclerotome progenitors divided at least once to give rise to one perivascular fibroblast (arrowheads) as well as several interstitial cells (arrows). A schematic representation of color-coded traced cells at the last time point is shown with perivascular fibroblasts indicated by asterisks. The corresponding time-lapse movie is shown in Movie S1. *n* = 6 embryos. (C) Quantification of the contribution of each sclerotome domain to perivascular fibroblasts. Sclerotome progenitors from each domain were quantified based on the final dorsoventral location of perivascular fibroblasts along each ISV. A given sclerotome progenitor can give rise to perivascular fibroblasts in only dorsal ISV, in only ventral ISV, or in both dorsal and ventral ISV as indicated in (A). The ventral sclerotome (combined) group includes progenitors from both the ventral sclerotome domain and

sclerotome derived notochord associated cells. *n* = 122 sclerotome progenitors from 6 embryos. Scale bar: 50 µm.

Fig. 3. Perivascular fibroblasts are distinct from pericytes. (A) Quantification of the number of perivascular fibroblasts and pericytes during development. The number of perivascular fibroblasts and pericytes were scored in *nkx3.1*$^{NTR\text{-}mCherry}$*; kdrl:EGFP* and *pdgfrb*$^{NTR\text{-}mCherry}$*; kdrl:EGFP* embryos, respectively. Each data point represents the average cell number of 8-10 ISVs from an individual embryo. Data are plotted with mean ± SEM indicated. *n* = 4-5 (*nkx3.1*$^{NTR\text{-}mCherry}$*; kdrl:EGFP*) and 11 (*pdgfrb*$^{NTR\text{-}mCherry}$*; kdrl:EGFP*) embryos at each time point. (B) *pdgfrb*$^{NTR\text{-}mCherry}$*; col1a2:GFP* embryos were imaged at 4 dpf to visualize perivascular fibroblasts and pericytes. No overlap in marker expression was observed between *pdgfrb*$^{NTR\text{-}mCherry}$-positive pericytes (red, arrows) and *col1a2:GFP*-positive perivascular fibroblasts (green, arrowheads). Unlike perivascular fibroblasts, pericytes also displayed elongated cellular processes (notched arrowheads). *n* = 14 embryos. (C) *pdgfrb*$^{NTR\text{-}mCherry}$*; kdrl:EGFP* embryos were imaged at 3 dpf to visualize individual pericytes (green, asterisks) with long cellular processes (notched arrowheads) that wrapped around the ISV (red). (D) Mosaic *col1a2*^{Kaede} line was imaged to visualize a single perivascular fibroblast (green, asterisks) associated with an ISV (red) in *col1a2*^{Kaede} ; *kdrl:mCherry* embryos at 3 dpf. Perivascular fibroblasts showed an overall globular morphology with shorter processes (notched arrowheads) wrapping loosely around the neighbouring ISV. Scale bars: (B) 25 µm; (C,D) 10 µm.

Fig. 4. Perivascular fibroblasts function as pericyte progenitors. (A) Snapshots from time-lapse imaging of *pdgfrb*$^{NTR\text{-}mCherry}$*; col1a2:GFP* embryos from 54 to 73 hpf. Newly differentiated pericytes were retrospectively traced to identify their cell of origin. The ISV is outlined by dotted lines at the first time point. One perivascular fibroblast (green, arrows) traced can be seen gradually upregulating *pdgfrb*$^{NTR\text{-}mCherry}$ expression and extending pericyte-like cellular processes (notched arrowheads). The time stamps are indicated in the hh:mm format. Schematic drawings of the merged images at each time point are shown at the bottom. The corresponding time-lapse movie is shown in Movie S2. *n* = 7 embryos. (B) Schematic showing experimental timeline of perivascular fibroblast ablation. *col1a2*$^{NTR\text{-}mCherry}$*; pdgfrb:GFP* embryos were incubated in either water or metronidazole (MTZ) from 1 to 3 dpf following which embryos was washed at 3 dpf and imaged at 4 dpf to visualize pericytes. (C) Representative images of water (left) or MTZ (right) treated *col1a2*$^{NTR\text{-}mCherry}$*; pdgfrb:GFP* embryos at 4 dpf. Compared to water-treated control embryos, MTZ-treated embryos showed complete ablation of mCherry^{+} cells with only residual mCherry^{+} debris (notched arrowheads). Fewer *pdgfrb:GFP*^{high} pericytes (arrowheads) can be seen in MTZ-treated embryos compared to water-treated controls. (D)

690 Quantification of the number of pericytes after perivascular fibroblast ablation. Pericytes were scored
691 based on high level expression of the *pdgfrb:GFP* reporter as shown in (C). Each data point
692 represents the average number of pericytes per ISV scored from 8-10 ISVs from an individual
693 embryo. *n* = 10 (water) and 23 (MTZ) embryos. Data are plotted as mean ± SEM. Statistics: Mann-
694 Whitney *U* test. Asterisk representation: p-value < 0.0001 (****). Scale bars: (A) 10 µm; (C) 50 µm.
695
696 **Fig. 5. Perivascular fibroblasts stabilize nascent blood vessels by collagen deposition.** (A)
697 Schematic of experimental protocol for early ablation of perivascular fibroblasts. *nkx3.1*$^{NTR\text{-}mCherry}$*;*
698 *kdrl:EGFP* embryos were incubated in either water or metronidazole (MTZ) from 38 to 62 hpf and
699 imaged to visualize ISV morphology. (B) Representative images showing water (left) and MTZ (right)
700 treated embryos. Water-treated control embryos had many mCherry^{+} cells (arrowheads), while MTZ
701 treatment resulted in complete ablation of mCherry^{+} cells with only mCherry^{+} debris (notched
702 arrowheads) remaining. MTZ-treated embryos showed visibly deformed ISV morphology with greater
703 variation in vessel diameter (arrows indicate the narrow region of ISVs) compared to uniform ISVs in
704 controls. (C) Quantification of ISV diameter variability in (B). ISV diameter was measured at 4
705 equidistant points along each ISV using the line tool in ImageJ. Mean diameter of each ISV was
706 calculated and standard deviation from the mean was plotted as a readout of diameter variability in
707 each ISV examined. MTZ-treated embryos showed significantly more variable ISVs compared to
708 water-treated controls. *n* = 115 ISVs from 14 embryos (water); 126 ISVs from 15 embryos (MTZ).
709 Results were graphed as mean ± SEM. Statistics: Mann-Whitney *U* test. Asterisk representation: p-
710 value < 0.0001 (****). (D) *nkx3.1*$^{NTR\text{-}mCherry}$ embryo were injected with the *UAS:Col1a2-GFP* plasmid
711 and imaged at 56 and 72 hpf. Many mCherry^{+}GFP^{+} perivascular fibroblasts (arrowheads) can be seen
712 surrounding the ISV. Numerous thin GFP^{+} collagen fibers (notched arrowheads) wrapped around the
713 ISV and the Col1a2-GFP protein deposition appeared to increase from 56 to 72 hpf. *n* = 16 embryos.
714 (E) *nkx3.1*$^{NTR\text{-}mCherry}$ embryos were injected with a low dose of the *UAS:Col1a2-GFP* plasmid and
715 imaged at 72 hpf. Col1a2-GFP deposition (notched arrowheads) around an ISV by a single
716 mCherry^{+}GFP^{+} perivascular fibroblast (arrowheads) can be seen. *n* = 16 embryos. Scale bars: (B) 50
717 µm; (D,E) 25 µm.
718
719 **Fig. 6. Characterization of collagen mutants.** (A) Embryos from intercrosses of *col1a2*$^{+/-}$ adults or
720 *col5a1*$^{+/-}$ adults were stained at 24 hpf by mRNA in situ hybridization with *col1a2* (left) or *col5a1* (right)
721 probes, respectively. Compared to wild type siblings, heterozygous mutants showed reduced staining,
722 and homozygous mutants displayed an almost complete loss of staining for both genes examined. *n* =
723 30 embryos for each staining. (B) *col5a1*$^{-/-}$ mutants but not wild-type siblings showed spontaneous

hemorrhage in the trunk (arrowhead) at 2 dpf. (C) Schematic of experimental protocol for phenotypic analysis of collagen mutants. Embryos from intercrosses of 1) *col1a2*$^{+/-}$ adults, 2) *col5a1*$^{+/-}$ adults, or 3) *col1a2*$^{+/-}$*; col5a1*$^{+/-}$ adults were incubated in either water or 0.6% methylcellulose (MC) and screened for the hemorrhage phenotype in the trunk from 48 to 80 hpf. All embryos were subsequently genotyped. (D) Quantification of hemorrhage penetrance of embryos from intercrosses of *col1a2*$^{+/-}$*; col5a1*$^{+/-}$ adults described in (C). The hemorrhage penetrance was calculated by dividing the number of embryos with the hemorrhage phenotype by the total number of embryos of the same genotype. *n* = 12 (*col1a2*$^{+/+}$*; col5a1*$^{+/+}$ + water); 9 (*col1a2*$^{+/+}$*; col5a1*$^{+/+}$ + MC); 12 (*col1a2*$^{+/+}$*; col5a1*$^{-/-}$ + water); 12 (*col1a2*$^{+/+}$*; col5a1*$^{-/-}$ + MC); 22 (*col1a2*$^{+/-}$*; col5a1*$^{-/-}$ + water); 27 (*col1a2*$^{+/-}$*; col5a1*$^{-/-}$ + MC); 12 (*col1a2*$^{-/-}$*; col5a1*$^{-/-}$ + water); and 18 (*col1a2*$^{-/-}$*; col5a1*$^{-/-}$ + MC) embryos. (E) *col1a2*$^{-/-}$*; col5a1*$^{-/-}$ embryos were incubated in water (top) or MC (bottom) for 3 hours at 2 dpf. MC-treated *col1a2*$^{-/-}$*; col5a1*$^{-/-}$ embryos showed an increase in the number of hemorrhage foci (arrowheads) compared to water-treated controls. Quantification of this result is shown in Fig S6D. (F) Embryos from crosses of *col1a2*$^{+/-}$*; col5a1*$^{+/-}$ and *col5a1*$^{+/-}$*; kdrl:EGFP* adults were incubated in the 0.6% methylcellulose solution at 48 hpf, and their ISVs were imaged at 53 hpf. *col5a1*$^{-/-}$*; kdrl:EGFP* embryos showed visible ISV constrictions (arrow) and broken ISVs (asterisk) compared to *col5a1*$^{+/+}$*; kdrl:EGFP* siblings. (G) Quantification of ISV diameter variability in embryos from crosses of *col1a2*$^{+/-}$*; col5a1*$^{+/-}$ and *col5a1*$^{+/-}$*; kdrl:EGFP* adults as described in (F). ISV diameter and variability were measured as described in Fig 5. *n* = 81 ISVs from 10 embryos (*col1a2*$^{+/+}$*; col5a1*$^{+/+}$*; kdrl:EGFP*); 20 ISVs from 3 embryos (*col1a2*$^{+/+}$*; col5a1*$^{-/-}$*; kdrl:EGFP*); and 34 ISVs from 4 embryos (*col1a2*$^{+/-}$*; col5a1*$^{-/-}$*; kdrl:EGFP*). Data are graphed as mean ± SEM. Statistics: Mann-Whitney *U* test. Asterisk representation: p-value < 0.05 (*); p-value < 0.005 (**); p-value < 0.0001 (****). Scale bars: (A) 250 μm; (B,E) 100 μm; (F) 50 μm.

Fig. 7. Model of perivascular fibroblasts in vascular stabilization in zebrafish. Perivascular fibroblasts, characterized by the expression of fibrillar collagens *col1a2* and *col5a1,* become associated with intersegmental vessels (ISVs) in the zebrafish trunk by 1.5 dpf. Perivascular fibroblasts deposit a network of collagen fibers to establish the vascular ECM and stabilize nascent ISVs at 2 dpf and continue to deposit collagen until at least 3 dpf. In the same time window, a subset of perivascular fibroblasts functions as pericyte progenitors. They gradually upregulate the expression of the classic pericyte marker *pdgfrb*, and develop elongated cellular processes. By 3 dpf, these 'pericyte progenitors' have completely differentiated into mature pericytes, showing robust *pdgfrb* expression distinct from *col1a2*$^{+}$ perivascular fibroblasts. Together, perivascular fibroblasts perform dual functions in vascular stabilization by depositing collagens to support nascent blood vessels and acting as pericyte progenitors.

SUPPLEMENTAL FIGURES

Fig. S1. Co-expression of *col1a2* and *col5a1* in perivascular fibroblasts. *kdrl:EGFP* embryos at 48 hpf were co-labeled with *col1a2* (red) and *col5a1* (green) by double fluorescent in situ hybridization followed by immunofluorescence labeling using the GFP antibody (blue). Co-expression of *col1a2* and *col5a1* is observed in perivascular fibroblasts (arrowheads) along EGFP$^+$ ISVs. *n* = 23 embryos. Scale bar: 50 μm.

Fig. S2. Developmental time-course of perivascular fibroblasts. *nkx3.1$^{NTR\text{-}mCherry}$; kdrl:EGFP* embryos were imaged at 26, 31, and 35 hpf to visualize different stages of perivascular fibroblast development. At 26 hpf, some *nkx3.1$^{NTR\text{-}mCherry}$* cells (arrowhead) were visible along the ventral half of ISV sprouts. As ISV lumenization became visible (asterisk) at 31 hpf, more *nkx3.1$^{NTR\text{-}mCherry}$* cells (arrowheads) appeared along ISVs. By 35 hpf, mCherry$^+$ cells (arrowheads) were present along the entire length of ISVs. Scale bar: 50 μm.

Fig. S3. Characterization of transgenic reporters. (A) *col1a2$^{NTR\text{-}mCherry}$; col1a2:GFP* embryos were imaged at 2 dpf. Due to the mosaic nature of both reporters, some perivascular fibroblasts were GFP$^+$mCherry$^+$ (white arrowheads), some GFP$^+$mCherry$^-$ (cyan arrowheads), and some GFP$^-$mCherry$^+$ (yellow arrowheads). *n* = 5 embryos. (B) *pdgfrb$^{NTR\text{-}mCherry}$; pdgfrb:GFP* embryos were imaged at 2 dpf (top panel) and 4 dpf (bottom panel). At 2 dpf, most perivascular fibroblasts were GFP$^+$mCherry$^-$ (white arrowheads) while a few cells were GFP$^+$mCherry$^+$ (cyan arrowheads). At 4 dpf, pericytes were GFP^{high}mCherry$^+$ (arrows) whereas perivascular fibroblasts were GFP^{low}mCherry$^-$ (arrowheads). *n* = 15 embryos. (C) *nkx3.1$^{NTR\text{-}mCherry}$; pdgfrb:GFP* embryos were imaged at 2 dpf. Perivascular fibroblasts (arrowheads) were positive for both *nkx3.1$^{NTR\text{-}mCherry}$* (red) and *pdgfrb:GFP* (green) reporters. *n* = 15 embryos. Scale bars: 50 μm.

Fig. S4. Late ablation of perivascular fibroblasts does not alter ISV morphology. (A) Schematic of experimental procedure for late perivascular fibroblast ablation. *col1a2$^{NTR\text{-}mCherry}$; kdrl:EGFP* embryos were incubated in either water or MTZ from 4 to 5 dpf and imaged to visualize ISV morphology. (B) Representative images showing water (left) and MTZ (right) treated embryos. Water-treated control embryos had many mCherry$^+$ cells (arrowheads), whereas MTZ treatment resulted in complete perivascular fibroblast ablation, with only mCherry$^+$ debris visible (notched arrowheads). No distinguishable difference in ISV morphology was visible between MTZ treated and control embryos. (C) Quantification of ISV diameter variability in (B). ISV diameter and variability measurements were

quantified as described in Fig 5. *n* = 103 ISVs from 9 embryos (water); 107 ISVs from 13 embryos (MTZ). Data are plotted as mean ± SEM. Statistics: Mann-Whitney *U* test. ns: not significant. Scale bar: (B) 50 μm.

Fig. S5. Generation of collagen mutants. (A) Sequencing chromatograms of *col1a2* WT and *col1a2*^{ca108} sequences. The sgRNA target sequence is underlined and the PAM motif is highlighted with a black box. The 1bp deletion in the *col1a2*^{ca108} sequence is denoted with an orange box. (B) Sequencing chromatograms of *col5a1* WT and *col5a1*^{ca109} sequences. The sgRNA target sequence is underlined and the PAM motif is highlighted with a black box. The 4bp deletion in the *col5a1*^{ca109} sequence is denoted with an orange box. (C) Alignment of *col1a2* WT and *col1a2*^{ca108} protein sequences. (D) Alignment of *col5a1* WT and *col5a1*^{ca109} protein sequences. Protein sequences were aligned using Clustal Omega (https://www.ebi.ac.uk/Tools/msa/clustalo/).

Fig. S6. Characterization of collagen mutants. (A) Distribution of genotypes in progeny of *col1a2*$^{+/-}$ intercrosses. Embryos from the mentioned crosses were grown and genotyped every 7 days from 7 dpf to 35 dpf to determine genotype distribution. Distribution of genotypes followed roughly Mendelian ratios at all stages examined. (B) Comparison of adult wild type and *col1a2*$^{-/-}$ siblings. (C) Distribution of genotypes in progeny of *col5a1*$^{+/-}$ intercrosses. Embryos from crosses of *col5a1*$^{+/-}$ adults were grown and genotyped at 3 day intervals from 5 dpf to 17 dpf. While the distribution of genotypes followed mendelian ratios at 5 and 8 dpf, *col5a1*$^{-/-}$ fish were completely absent at 14 and 17 dpf. (D) Quantification of hemorrhage severity in collagen mutants shown in Fig 5D and 5E. Hemorrhage severity was scored by counting the number of visible hemorrhage foci present in the trunk. Fish with no visible hemorrhage were counted as 0. Increased physical stress in the viscous MC solution resulted in an increase in hemorrhage severity across mutants with different genotypes. *n* = 12 (*col1a2*$^{+/+}$*; col5a1*$^{-/-}$ + water); 11 (*col1a2*$^{+/+}$*; col5a1*$^{-/-}$ + MC); 20 (*col1a2*$^{+/-}$*; col5a1*$^{-/-}$ + water); 26 (*col1a2*$^{+/-}$*; col5a1*$^{-/-}$ + MC); 12 (*col1a2*$^{-/-}$*; col5a1*$^{-/-}$ + water); and 18 (*col1a2*$^{-/-}$*; col5a1*$^{-/-}$ + MC) embryos. Results were graphed as mean ± SEM. Statistics: Mann-Whitney *U* test. Asterisk representation: p-value < 0.05 (*); p-value < 0.0001 (****). Scale bar: (B) 2 mm.

Movie S1. Perivascular fibroblasts originate from the sclerotome. *nkx3.1*$^{NTR\text{-}mCherry}$*; kdrl:EGFP* embryos were imaged from 25 hpf to 49.5 hpf at ~8 minute intervals (7 min 58 sec) with time stamps indicated in the hh:mm format. Perivascular fibroblasts along ISVs were retrospectively traced to determine their cell of origin. One cell from the ventral sclerotome domain (cyan arrows) and one cell from sclerotome derived notochord associated cells (yellow arrows) were traced over 24.5 hours with

826 their daughter cells indicated by the same colored arrows/arrowheads. Both sclerotome progenitors
827 divided at least once to give rise to one perivascular fibroblast (arrowheads) as well as several
828 interstitial cells (arrows). Snapshots of this time-lapse movie are shown in Fig 2B. *n* = 6 embryos.
829 Scale bar: 50 μm.
830
831 **Movie S2. Perivascular fibroblasts function as pericyte progenitors.** *pdgfrb*$^{NTR\text{-}mCherry}$*; col1a2:GFP*
832 embryos were imaged from 54 hpf to 73 hpf at 6 minute intervals with time stamps indicated in the
833 hh:mm format. Newly differentiated pericytes were retrospectively traced to identify their cell of origin.
834 One perivascular fibroblast (green, arrows) traced can be seen gradually upregulating *pdgfrb*$^{NTR\text{-}mCherry}$
835 expression and extending pericyte-like cellular processes (notched arrowheads). Snapshots of this
836 time-lapse movie are shown in Fig 4A. *n* = 7 embryos. Scale bar: 25 μm.
837
838 **Movie S3. Perivascular fibroblasts function as pericyte progenitors.** *nkx3.1*$^{NTR\text{-}mCherry}$*; pdgfrb:GFP*
839 embryos were imaged from 54 hpf to 76 hpf at 15 minute intervals with time stamps indicated in the
840 hh:mm format. Two perivascular fibroblasts traced (arrows) can be seen gradually upregulating
841 *pdgfrb:GFP* expression and extending pericyte-like cellular processes (notched arrowheads). Note
842 that one of the traced cells (top arrows) migrated away from the ISV at 15:15. *n* = 16 embryos. Scale
843 bar: 25 μm.

REFERENCES

1. Xu J, Shi G-P. Vascular wall extracellular matrix proteins and vascular diseases. Biochim Biophys Acta. 2014;(11):2106–19.
2. Murakami M, Simons M. Regulation of vascular integrity. Journal of Molecular Medicine. 2009;87:571–82.
3. Michel JB, Martin-Ventura JL, Egido J, Sakalihasan N, Treska V, Lindholt J, et al. Novel aspects of the pathogenesis of aneurysms of the abdominal aorta in humans. Cardiovasc Res. 2011;90(1):18–27.
4. Sakalihasan N, Michel JB, Katsargyris A, Kuivaniemi H, Defraigne JO, Nchimi A, et al. Abdominal aortic aneurysms. Nature Reviews Disease Primers. 2018;4:34.
5. Qureshi AI, Mendelow AD, Hanley DF. Intracerebral haemorrhage. The Lancet. 2009;373:1632–44.
6. Brisman JL, Song JK, Newell DW. Cerebral aneurysms. The New England Journal of Medicine. 2006;355:928-39
7. Dejana E, Tournier-Lasserve E, Weinstein BM. The Control of Vascular Integrity by Endothelial Cell Junctions: Molecular Basis and Pathological Implications Developmental Cell. 2009. 16:209–21.
8. Gaengel K, Genové G, Armulik A, Betsholtz C. Endothelial-mural cell signaling in vascular development and angiogenesis. Arterioscler Thromb Vasc Biol. 2009 May 1;29(5):630–8.
9. Levéen P, Pekny M, Gebre-Medhin S, Swolin B, Larsson E, Betsholtz C. Mice deficient for PDGF B show renal, cardiovascular, and hematological abnormalities. Genes Dev. 1994;8(16):1875–87.
10. Lindahl P, Johansson BR, Levéen P, Betsholtz C. Pericyte loss and microaneurysm formation in PDGF-B-deficient mice. Science. 1997 Jul 11;277(5323):242–5.
11. Soriano P. Abnormal kidney development and hematological disorders in PDGF β- receptor mutant mice. Genes Dev. 1994;8(16):1888–96.
12. Hellström M, Gerhardt H, Kalén M, Li X, Eriksson U, Wolburg H, et al. Lack of pericytes leads to endothelial hyperplasia and abnormal vascular morphogenesis. J Cell Biol. 2001 Feb 5;152(3):543–53.
13. Bjarnegård M, Enge M, Norlin J, Gustafsdottir S, Fredriksson S, Abramsson A, et al. Endothelium-specific ablation of PDGFB leads to pericyte loss and glomerular, cardiac and placental abnormalities. Development. 2004 Apr;131(8):1847–57.
14. Rhodes JM, Simons M. The extracellular matrix and blood vessel formation: Not just a scaffold:

878 Angiogenesis Review Series. Journal of Cellular and Molecular Medicine. 2007;11:176–205.
879 15. Löhler J, Timpl R, Jaenisch R. Embryonic lethal mutation in mouse collagen I gene causes
880 rupture of blood vessels and is associated with erythropoietic and mesenchymal cell death.
881 Cell. 1984;38:597–607.
882 16. Liu X, Wu H, Byrne M, Krane S, Jaenisch R. Type III collagen is crucial for collagen I
883 fibrillogenesis and for normal cardiovascular development. Proc Natl Acad Sci U S A. 1997 Mar
884 4;94(5):1852–6.
885 17. Pöschl E, Schlötzer-Schrehardt U, Brachvogel B, Saito K, Ninomiya Y, Mayer U. Collagen IV is
886 essential for basement membrane stability but dispensable for initiation of its assembly during
887 early development. Development. 2004 Apr;131(7):1619–28.
888 18. Thyboll J, Kortesmaa J, Cao R, Soininen R, Wang L, Iivanainen A, et al. Deletion of the
889 Laminin 4 Chain Leads to Impaired Microvessel Maturation. Mol Cell Biol. 2002 Feb
890 15;22(4):1194–202.
891 19. Malfait F. Vascular aspects of the Ehlers-Danlos Syndromes. Matrix Biol. 2017
892 20. Yamazaki T, Mukouyama Y. Tissue Specific Origin, Development, and Pathological
893 Perspectives of Pericytes. Front Cardiovasc Med. 2018 June;5:1–6.
894 21. Holm A, Heumann T, Augustin HG. Microvascular Mural Cell Organotypic Heterogeneity and
895 Functional Plasticity.Trends in Cell Biology. 2018;28(4).
896 22. Armulik A, Genové G, Betsholtz C. Pericytes: Developmental, Physiological, and Pathological
897 Perspectives, Problems, and Promises. Dev Cell. 2011 Aug 16;21(2):193–215.
898 23. Majesky MW. Developmental basis of vascular smooth muscle diversity. Arteriosclerosis,
899 Thrombosis, and Vascular Biology. Arterioscler Thromb Vasc Biol; 2007; 27:1248–58.
900 24. Crisan M, Corselli M, Chen WCW, Péault B. Perivascular cells for regenerative medicine. J Cell
901 Mol Med. 2012 Dec;16(12):2851–60.
902 25. Soderblom C, Luo X, Blumenthal E, Bray E, Lyapichev K, Ramos J, et al. Brief
903 Communications Perivascular Fibroblasts Form the Fibrotic Scar after Contusive Spinal Cord
904 Injury. 2013; 33(34):13882-87.
905 26. Guillemin GJ, Brew BJ. Microglia, macrophages, perivascular macrophages, and pericytes: a
906 review of function and identification. J Leukoc Biol. 2004 Mar 1;75(3):388–97.
907 27. Mato M, Ookawara S, Aikawa E, Kawasaki K. Studies on fluorescent granular perithelium
908 (F.G.P.) of rat cerebral cortex - especially referring to morphological changes in aging. Anat
909 Anz. 1981;149(5):486–501.
910 28. Galanternik MV, Castranova D, Gore A V., Blewett NH, Jung HM, Stratman AN, et al. A novel
911 perivascular cell population in the zebrafish brain. Elife. 2017 Apr 11;6:e24369.

29. Macvicar BA, Newman EA. Astrocyte regulation of blood flow in the brain. Cold Spring Harb Perspect Biol. 2015;7(5):1–15.
30. Marques S, Zeisel A, Codeluppi S, Van Bruggen D, Falcão AM, Xiao L, et al. Oligodendrocyte heterogeneity in the mouse juvenile and adult central nervous system. Science. 2016 Jun 10;352(6291):1326–9.
31. Zeisel A, Hochgerner H, Lönnerberg P, Johnsson A, Memic F, van der Zwan J, et al. Molecular Architecture of the Mouse Nervous System. Cell. 2018 Aug 9;174(4):999-1014.e22.
32. Saunders A, Macosko EZ, Wysoker A, Goldman M, Krienen FM, de Rivera H, et al. Molecular Diversity and Specializations among the Cells of the Adult Mouse Brain. Cell. 2018 Aug 9;174(4):1015-1030.e16.
33. Vanlandewijck M, He L, Mäe MA, Andrae J, Ando K, Del Gaudio F, et al. A molecular atlas of cell types and zonation in the brain vasculature. Nature. 2018 Feb 14;554(7693):475–80.
34. Kelly KK, Macpherson AM, Grewal H, Strnad F, Jones JW, Yu J, et al. Col1a1+ perivascular cells in the brain are a source of retinoic acid following stroke. BMC Neurosci. 2016;17:49.
35. Fernández-Klett F, Potas JR, Hilpert D, Blazej K, Radke J, Huck J, et al. Early loss of pericytes and perivascular stromal cell-induced scar formation after stroke. J Cereb Blood Flow Metab. 2013 Mar;33(3):428–39.
36. Göritz C, Dias DO, Tomilin N, Barbacid M, Shupliakov O, Frisén J. A pericyte origin of spinal cord scar tissue. Science. 2011 Jul 8;333(6039):238–42.
37. Makihara N, Arimura K, Ago T, Tachibana M, Nishimura A, Nakamura K, et al. Involvement of platelet-derived growth factor receptor β in fibrosis through extracellular matrix protein production after ischemic stroke. Exp Neurol. 2015 Feb 1;264:127–34.
38. Gore A V., Monzo K, Cha YR, Pan W, Weinstein BM. Vascular development in the zebrafish. Cold Spring Harb Perspect Med. 2012;2(5).
39. Howe K, Clark MD, Torroja CF, Torrance J, Berthelot C, Muffato M, et al. The zebrafish reference genome sequence and its relationship to the human genome. Nature. 2013 Apr 25;496(7446):498–503.
40. Yahn SL, Li J, Goo I, Gao H, Brambilla R, Lee JK. Fibrotic scar after experimental autoimmune encephalomyelitis inhibits oligodendrocyte differentiation. Neurobiol Dis [Internet]. 2020 Feb;134:104674.
41. Chico TJA, Ingham PW, Crossman DC. Modeling Cardiovascular Disease in the Zebrafish. Trends in Cardiovascular Medicine. Trends Cardiovasc Med; 2008;18:150–5.
42. Isogai S, Horiguchi M, Weinstein BM. The vascular anatomy of the developing zebrafish: An atlas of embryonic and early larval development. Dev Biol. 2001 Feb 15;230(2):278–301.

946 43. Santoro MM, Pesce G, Stainier DY. Characterization of vascular mural cells during zebrafish
947 development. Mech Dev. 2009 Aug;126(8–9):638–49.
948 44. Isogai S, Lawson ND, Torrealday S, Horiguchi M, Weinstein BM. Angiogenic network formation
949 in the developing vertebrate trunk. Development. 2003 Nov 1;130(21):5281–90.
950 45. Ando K, Fukuhara S, Izumi N, Nakajima H, Fukui H, Kelsh RN, et al. Clarification of mural cell
951 coverage of vascular endothelial cells by live imaging of zebrafish. Development. 2016 Apr
952 15;143(8):1328–39.
953 46. Ma RC, Jacobs CT, Sharma P, Kocha KM, Huang P. Stereotypic generation of axial tenocytes
954 from bipartite sclerotome domains in zebrafish. Moens C, editor. PLOS Genet. 2018 Nov
955 2;14(11):e1007775.
956 47. Olson LE, Soriano P. PDGFRβ signaling regulates mural cell plasticity and inhibits fat
957 development. Dev Cell. 2011 Jun 14;20(6):815–26.
958 48. Hellström, M., Kalen, M., Lindahl, P., Abramsson, A., Betsholtz, C. Role of PDGF-B and950PDGFR-β in
959 recruitment of vascular smooth muscle cells and pericytes during embryonic blood vessel formation in
960 the mouse.Ddevelopment. 1999; 126:3047-3055.
961 49. Sharma P, Ruel TD, Kocha KM, Liao S, Huang P. Single cell dynamics of embryonic muscle
962 progenitor cells in zebrafish. Dev. 2019 Jul 1;146(14).
963 50. Stratman AN, Pezoa SA, Farrelly OM, Castranova D, Dye LE, Butler MG, et al. Interactions
964 between mural cells and endothelial cells stabilize the developing zebrafish dorsal aorta.
965 Development. 2017 Jan 1;144(1):115–27.
966 51. Curado S, Stainier DYR, Anderson RM. Nitroreductase-mediated cell/tissue ablation in
967 zebrafish: A spatially and temporally controlled ablation method with applications in
968 developmental and regeneration studies. Nat Protoc. 2008 May;3(6):948–54.
969 52. Morris JL, Cross SJ, Lu Y, Kadler KE, Lu Y, Dallas SL, et al. Live imaging of collagen
970 deposition during skin development and repair in a collagen I - GFP fusion transgenic zebrafish
971 line. Dev Biol. 2018;441(1):4–11.
972 53. Gagnon JA, Valen E, Thyme SB, Huang P, Ahkmetova L, Pauli A, et al. Efficient Mutagenesis
973 by Cas9 Protein-Mediated Oligonucleotide Insertion and Large-Scale Assessment of Single-
974 Guide RNAs. Riley B, editor. PLoS One. 2014 May 29;9(5):e98186.
975 54. Fisher S, Jagadeeswaran P, Halpern ME. Radiographic analysis of zebrafish skeletal defects.
976 Dev Biol. 2003 Dec 1;264(1):64–76.
977 55. Gistelinck C, Kwon RY, Malfait F, Symoens S, Harris MP, Henke K, et al. Zebrafish type I
978 collagen mutants faithfully recapitulate human type I collagenopathies. Proc Natl Acad Sci U S
979 A. 2018 Aug 21;115(34):E8037–46.

980 56. Hall TE, Bryson-Richardson RJ, Berger S, Jacoby AS, Cole NJ, Hollway GE, et al. The
981 zebrafish candyfloss mutant implicates extracellular matrix adhesion failure in laminin α2-
982 deficient congenital muscular dystrophy. Proc Natl Acad Sci U S A. 2007 Apr 24;104(17):7092–
983 7.
984 57. Ando K, Wang W, Peng D, Chiba A, Lagendijk AK, Barske L, et al. Peri-arterial specification of
985 vascular mural cells from naïve mesenchyme requires Notch signaling. 2019; 146(2):dev165589.
986 58. Etchevers HC, Vincent C, Le Douarin NM, Couly GF. The cephalic neural crest provides
987 pericytes and smooth muscle cells to all blood vessels of the face and forebrain. Development.
988 2001;128(7):1059–68.
989 59. Bergwerff M, Verberne ME, DeRuiter MC, Poelmann RE, Gittenberger-de Groot AC. Neural
990 crest cell contribution to the developing circulatory system implications for vascular
991 morphology? Circ Res. 1998 Feb 9;82(2):221–31.
992 60. Wang Y, Pan Luyuan, Moens Cecilia B., Appel BRuce. Notch3 establishes brain vascular
993 integrity by regulating pericyte number. Development. 2014;141:1-11.
994 61. Domenga V, Fardoux P, Lacombe P, Monet M, Maciazek J, Krebs LT, et al. Notch3 is required
995 for arterial identity and maturation of vascular smooth muscle cells. Genes Dev. 2004 Nov
996 15;18(22):2730–5.
997 62. Liu H, Zhang W, Kennard S, Caldwell RB, Lilly B. Notch3 is critical for proper angiogenesis and
998 mural cell investment. Circ Res. 2010 Oct 1;107(7):860–70.
999 63. Kofler NM, Cuervo H, Uh MK, Murtomäki A, Kitajewski J. Combined deficiency of Notch1 and
1000 Notch3 causes pericyte dysfunction, models CADASIL, and results in arteriovenous
1001 malformations. Sci Rep. 2015;5(June):1–13.
1002 64. Ton Q V, Leino D, Mowery SA, Bredemeier NO, Lafontant PJ, Lubert A, et al. Collagen
1003 COL22A1 maintains vascular stability and mutations in COL22A1 are potentially associated
1004 with intracranial aneurysms. 2018;11:dmm033654.
1005 65. Ricard-Blum S. The Collagen Family. Cold Spring Harb Perspect Biol. 2011;3(1):1–19.
1006 66. Mak KM, Png CYM, Lee DJ. Type V Collagen in Health, Disease, and Fibrosis. Anat Rec.
1007 2016;299(5):613–29.
1008 67. Bretaud S, Nauroy P, Malbouyres M, Ruggiero F. Fishing for collagen function: About
1009 development, regeneration and disease. Semin Cell Dev Biol. 2019 May 1;89:100–8.
1010 68. De Paepe A, Malfait F. Bleeding and bruising in patients with Ehlers-Danlos syndrome and
1011 other collagen vascular disorders. Br J Haematol. 2004;127:491–500.
1012 69. Aszódi A, Legate KR, Nakchbandi I, Fässler R. What Mouse Mutants Teach Us About
1013 Extracellular Matrix Function. Annu Rev Cell Dev Biol. 2006 Nov;22(1):591–621.

70. Wenstrup RJ, Florer JB, Brunskill EW, Bell SM, Chervoneva I, Birk DE. Type V collagen controls the initiation of collagen fibril assembly. J Biol Chem. 2004 Dec 17;279(51):53331–7.
71. Dias DO, Kim H, Holl D, Werne Solnestam B, Lundeberg J, Carlén M, et al. Reducing Pericyte-Derived Scarring Promotes Recovery after Spinal Cord Injury. Cell. 2018;173(1):153-165.e22.
72. Choi J, Dong L, Ahn J, Dao D, Hammerschmidt M, Chen JN. FoxH1 negatively modulates flk1 gene expression and vascular formation in zebrafish. Dev Biol. 2007 Apr 15;304(2):735–44.
73. Proulx K, Lu A, Sumanas S. Cranial vasculature in zebrafish forms by angioblast cluster-derived angiogenesis. Dev Biol. 2010 Dec 1;348(1):34–46.
74. Whitesell TR, Chrystal PW, Ryu JR, Munsie N, Grosse A, French CR, et al. foxc1 is required for embryonic head vascular smooth muscle differentiation in zebrafish. Dev Biol. 2019 Sep 1;453(1):34–47.
75. Davison JM, Akitake CM, Goll MG, Rhee JM, Gosse N, Baier H, et al. Transactivation from Gal4-VP16 transgenic insertions for tissue-specific cell labeling and ablation in zebrafish. Dev Biol. 2007 Apr 15;304(2):811–24.
76. Montague TG, Cruz JM, Gagnon JA, Church GM, Valen E. CHOPCHOP: A CRISPR/Cas9 and TALEN web tool for genome editing. Nucleic Acids Res. 2014 Jul 1;42(W1).
77. Schindelin J, Arganda-Carreras I, Frise E, Kaynig V, Longair M, Pietzsch T, et al. Fiji: An open-source platform for biological-image analysis. Nature Methods. 2012;9:676–82.

Figure 1

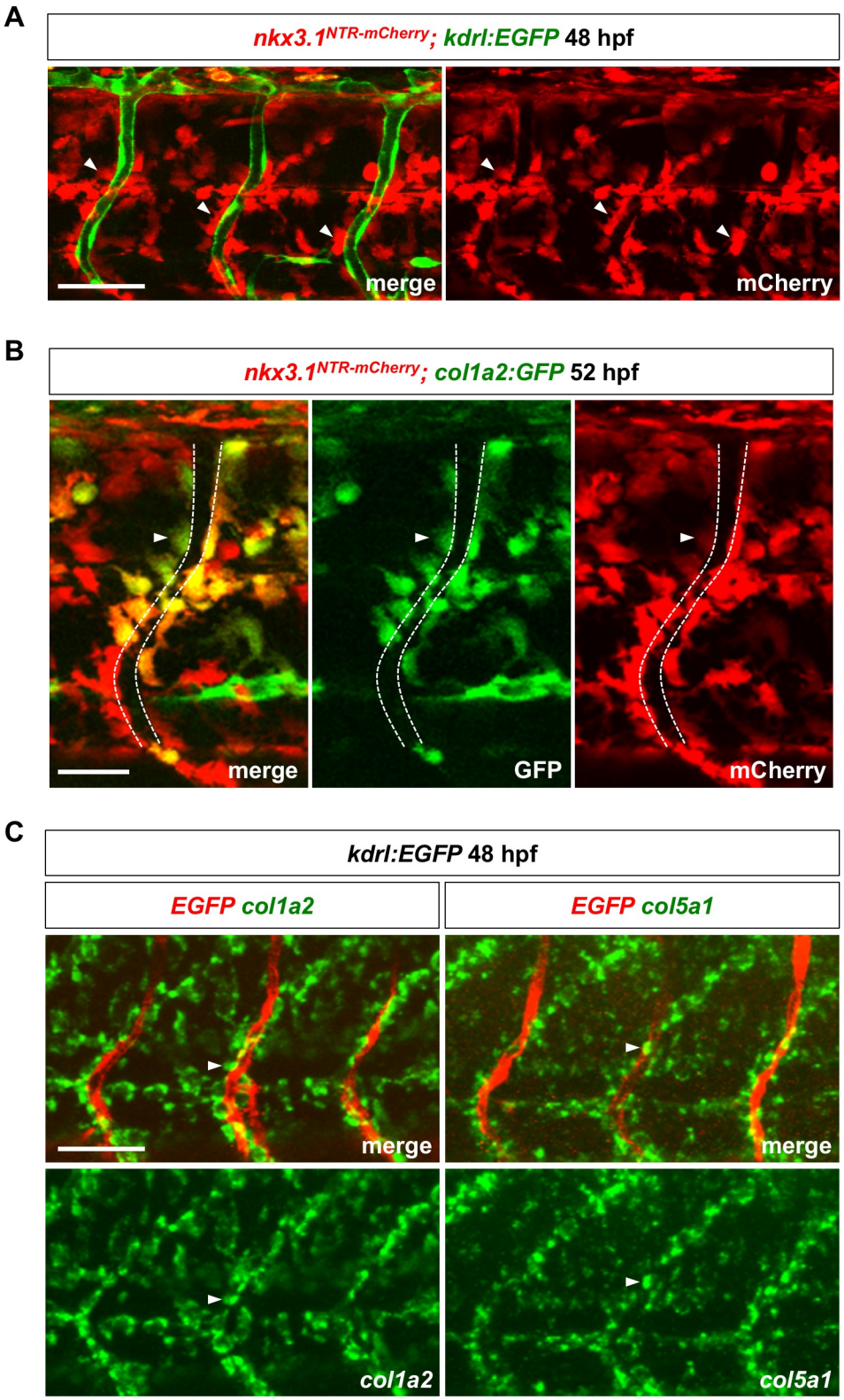
A
nkx3.1NTR-mCherry; kdrl:EGFP 48 hpf
merge
mCherry
B
nkx3.1NTR-mCherry; col1a2:GFP 52 hpf
merge
GFP
mCherry
C
kdrl:EGFP 48 hpf
EGFP col1a2
EGFP col5a1
merge
merge
col1a2
col5a1

Figure 2

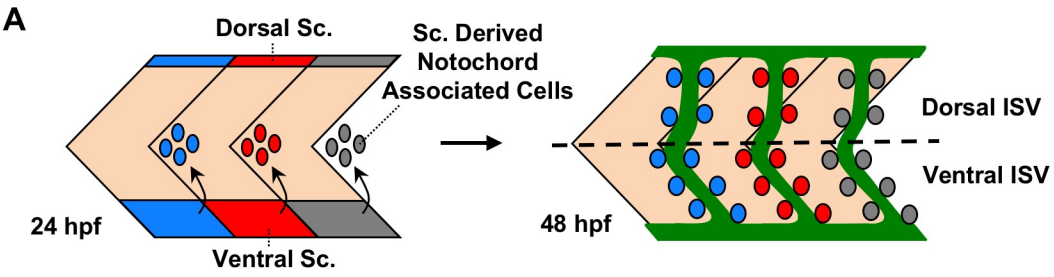
A
Dorsal Sc.
Sc. Derived
Notochord
Associated Cells
Dorsal ISV
Ventral ISV
24 hpf
48 hpf
Ventral Sc.

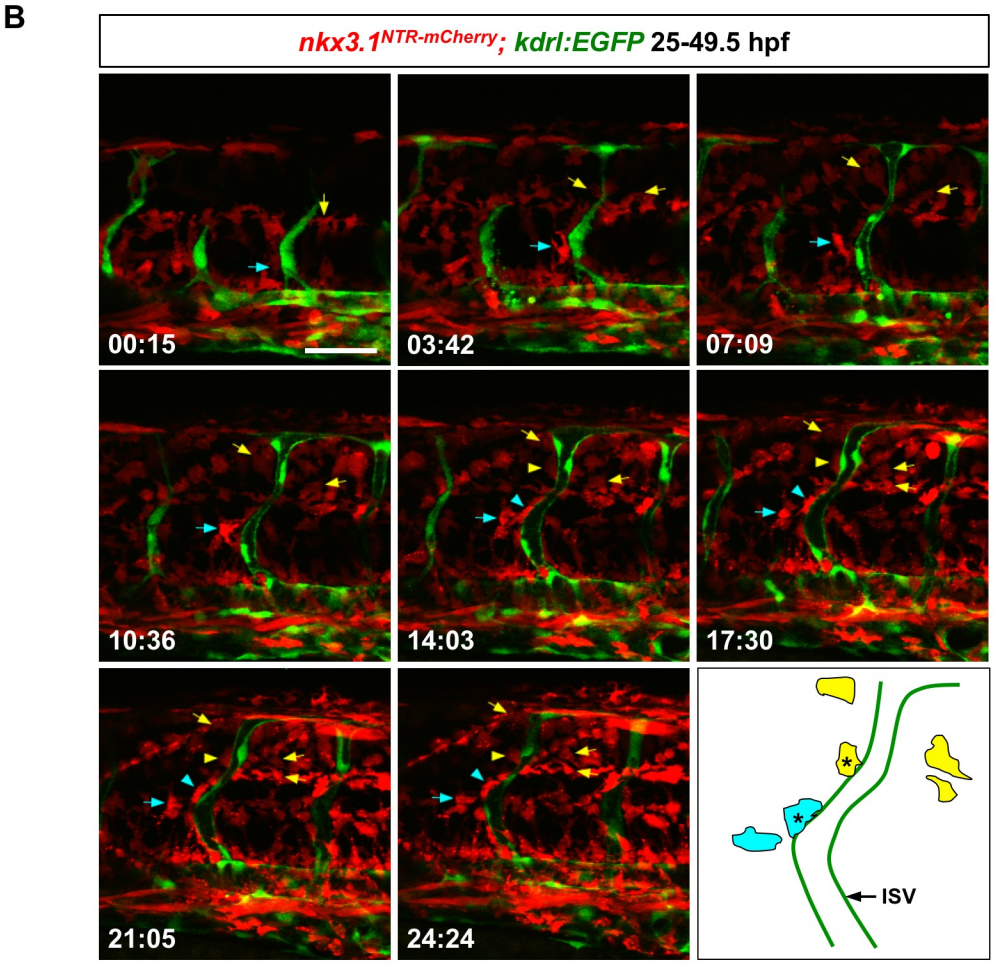
B
nkx3.1NTR-mCherry; kdrl:EGFP 25-49.5 hpf
00:15
03:42
07:09
10:36
14:03
17:30
21:05
24:24
ISV

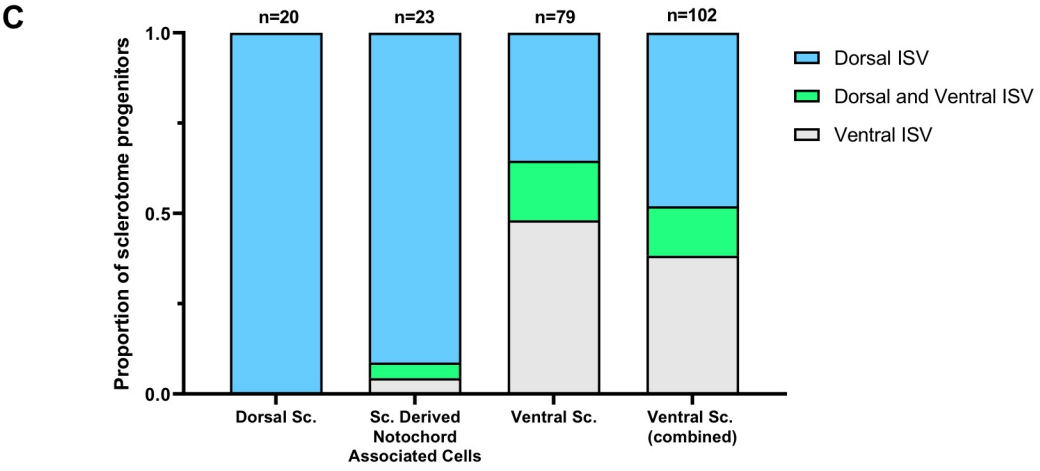
C
n=20
n=23
n=79
n=102
1.0
0.5
0.0
Proportion of sclerotome progenitors
Dorsal ISV
Dorsal and Ventral ISV
Ventral ISV
Dorsal Sc.
Sc. Derived Notochord Associated Cells
Ventral Sc.
Ventral Sc. (combined)

Figure 3

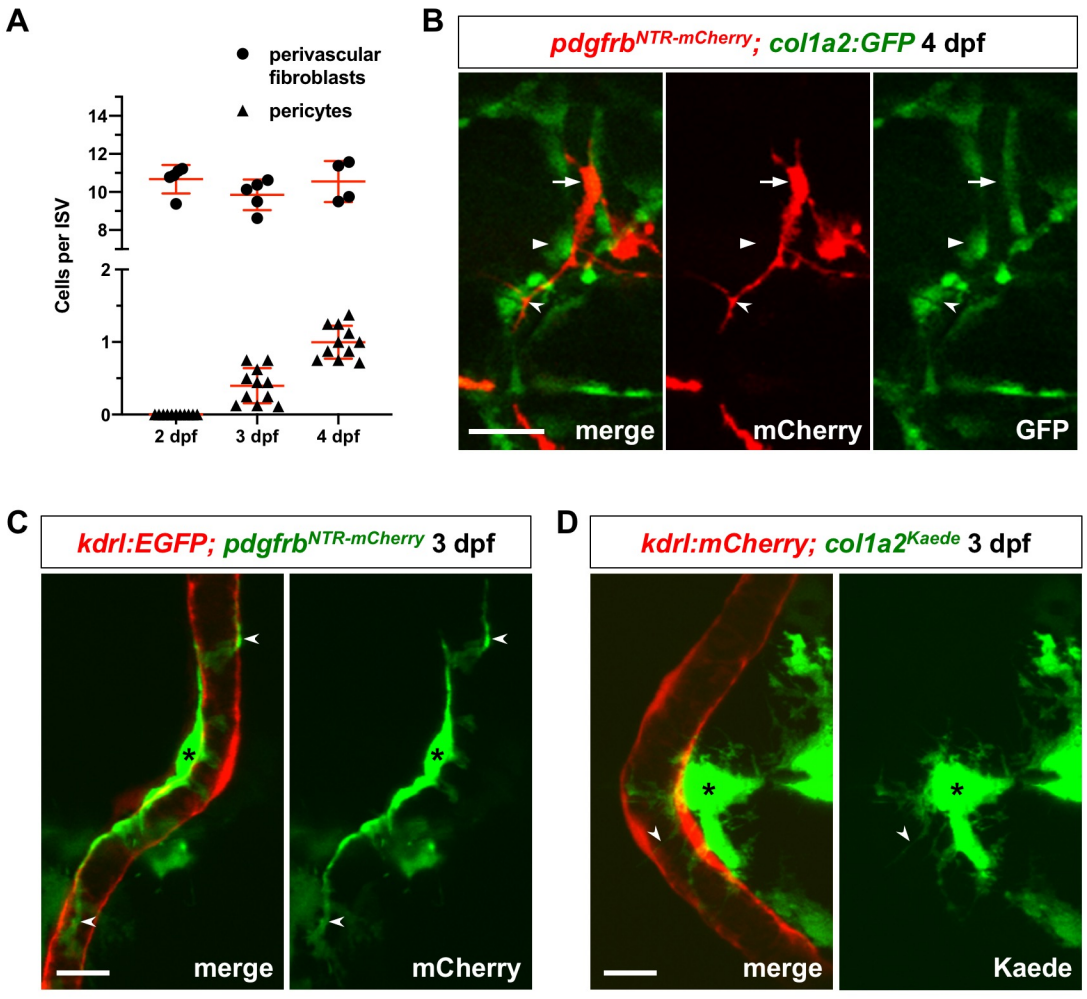
A
perivascular fibroblasts
pericytes
Cells per ISV
14
12
10
8
2
1
0
2 dpf
3 dpf
4 dpf
B
pdgfrb^NTR-mCherry; col1a2:GFP 4 dpf
merge
mCherry
GFP
C
kdrl:EGFP; pdgfrb^NTR-mCherry 3 dpf
merge
mCherry
D
kdrl:mCherry; col1a2^Kaede 3 dpf
merge
Kaede

Figure 4

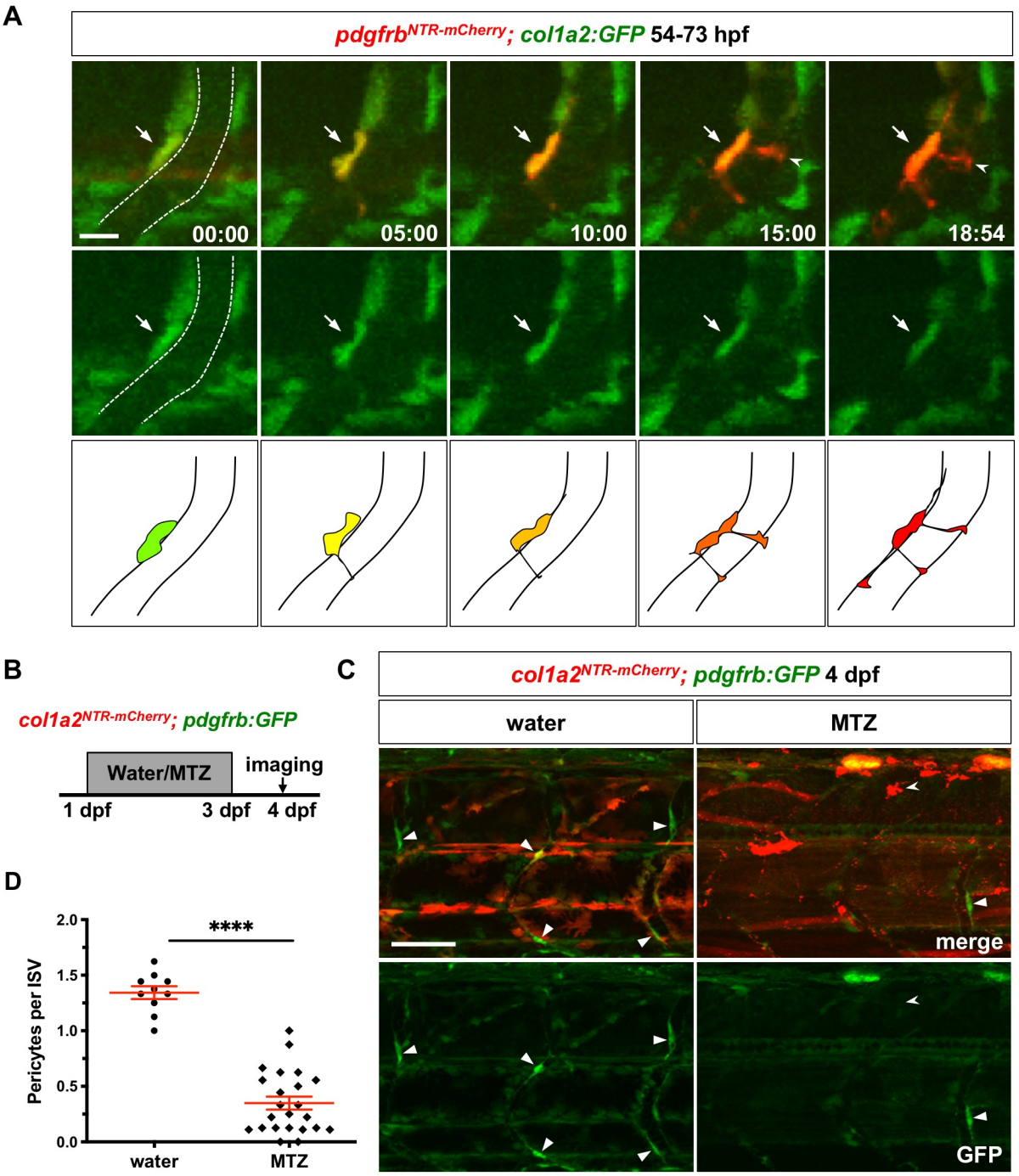
A
pdgfrb^NTR-mCherry; col1a2:GFP 54-73 hpf
00:00
05:00
10:00
15:00
18:54
B
col1a2^NTR-mCherry; pdgfrb:GFP
Water/MTZ
imaging
1 dpf
3 dpf
4 dpf
C
col1a2^NTR-mCherry; pdgfrb:GFP 4 dpf
water
MTZ
merge
GFP
D
Pericytes per ISV
2.0
1.5
1.0
0.5
0.0
****
water
MTZ

Figure 5

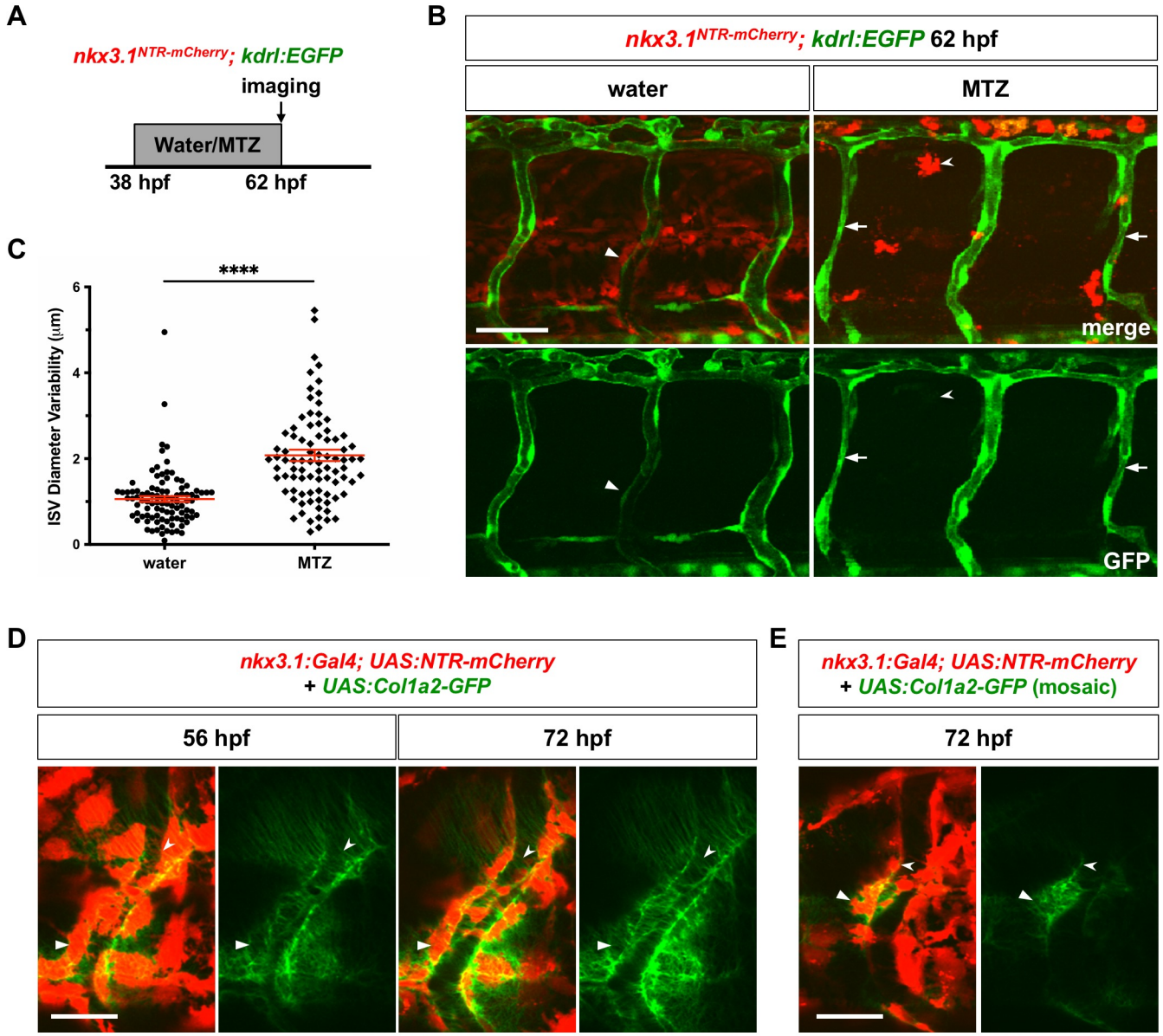
A
nkx3.1NTR-mCherry; kdrl:EGFP
imaging
Water/MTZ
38 hpf
62 hpf
B
nkx3.1NTR-mCherry; kdrl:EGFP 62 hpf
water
MTZ
merge
GFP
C
****
ISV Diameter Variability (μm)
6
4
2
0
water
MTZ
D
nkx3.1:Gal4; UAS:NTR-mCherry
+ UAS:Col1a2-GFP
56 hpf
72 hpf
E
nkx3.1:Gal4; UAS:NTR-mCherry
+ UAS:Col1a2-GFP (mosaic)
72 hpf

Figure 6

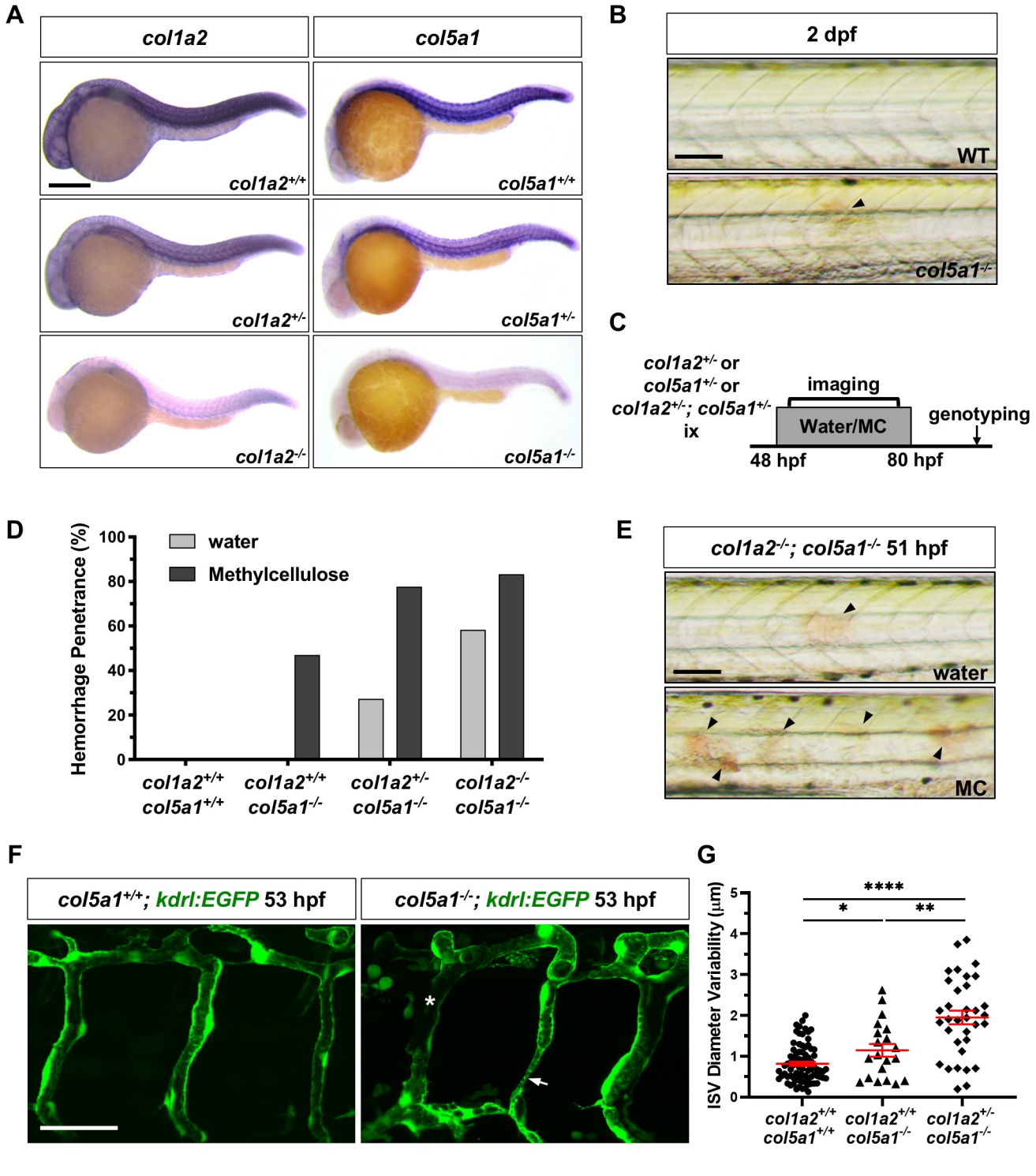
A
col1a2
col5a1
col1a2+/+
col5a1+/+
col1a2+/-
col5a1+/-
col1a2-/-
col5a1-/-
B
2 dpf
WT
col5a1-/-
C
col1a2+/- or
col5a1+/- or
col1a2+/-; col5a1+/-
ix
imaging
Water/MC
genotyping
48 hpf
80 hpf
D
Hemorrhage Penetrance (%)
100
80
60
40
20
0
water
Methylcellulose
col1a2+/+ col5a1+/+
col1a2+/+ col5a1-/-
col1a2+/- col5a1-/-
col1a2-/- col5a1-/-
E
col1a2-/-; col5a1-/- 51 hpf
water
MC
F
col5a1+/+; kdrl:EGFP 53 hpf
col5a1-/-; kdrl:EGFP 53 hpf
G
ISV Diameter Variability (μm)
5
4
3
2
1
0
****
*
**
col1a2+/+ col5a1+/+
col1a2+/+ col5a1-/-
col1a2+/- col5a1-/-

Figure 7

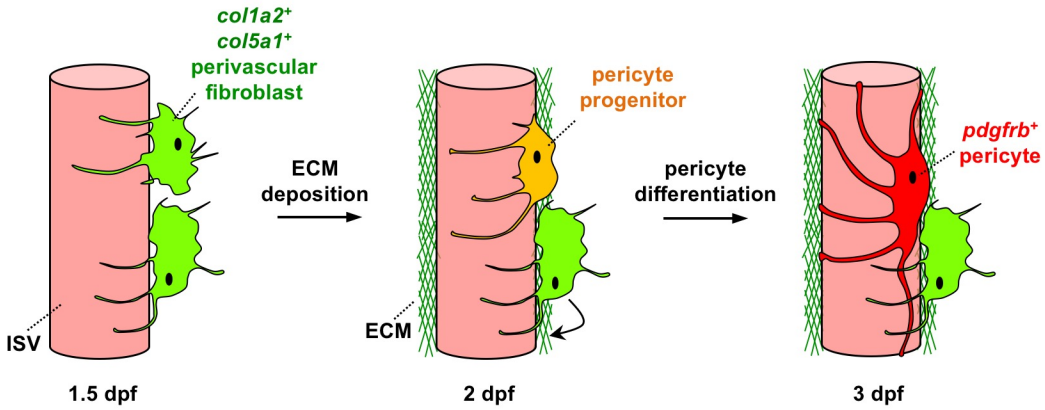
col1a2+
col5a1+
perivascular
fibroblast
ISV
1.5 dpf
ECM
deposition
pericyte
progenitor
ECM
2 dpf
pericyte
differentiation
pdgfrb+
pericyte
3 dpf

Figure S1

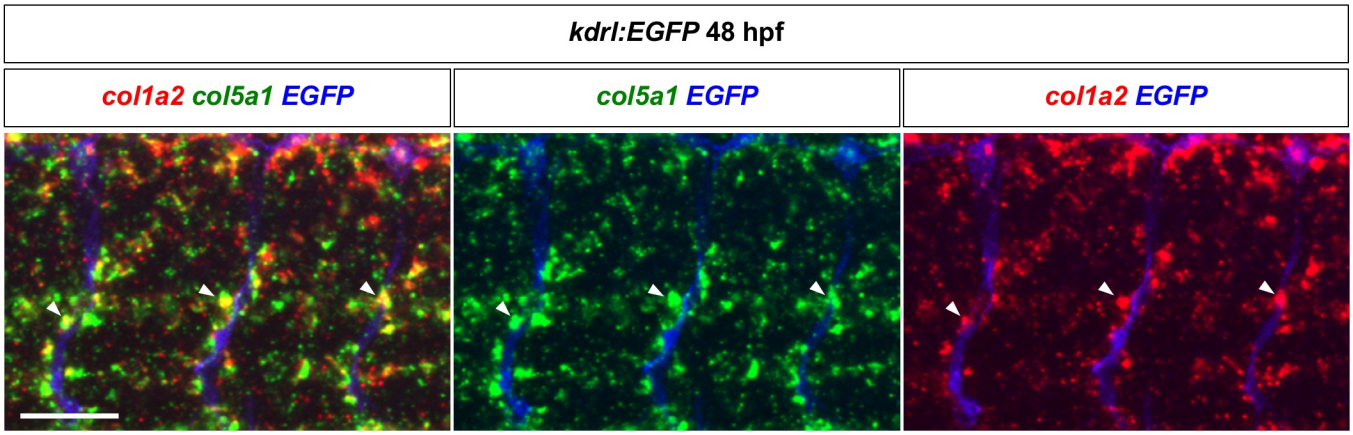

Figure S2

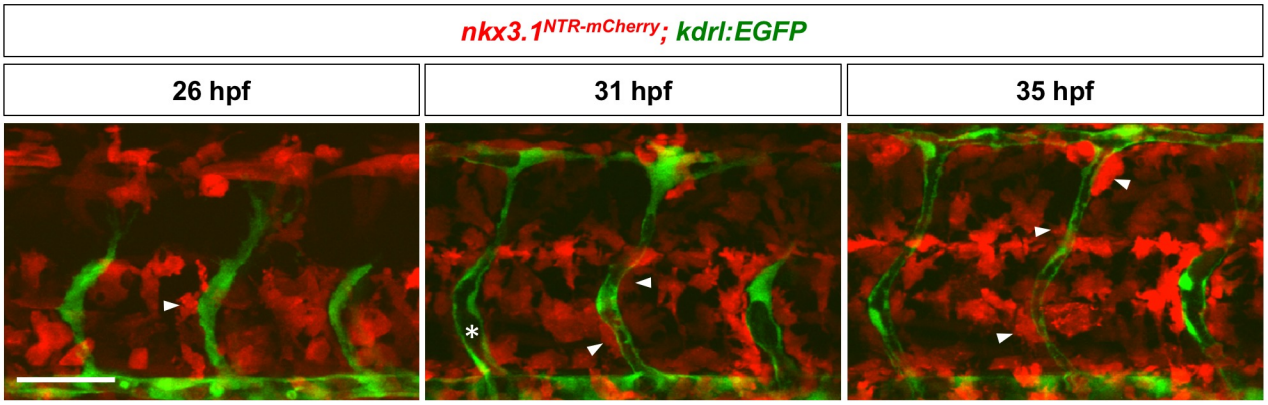

Figure S3

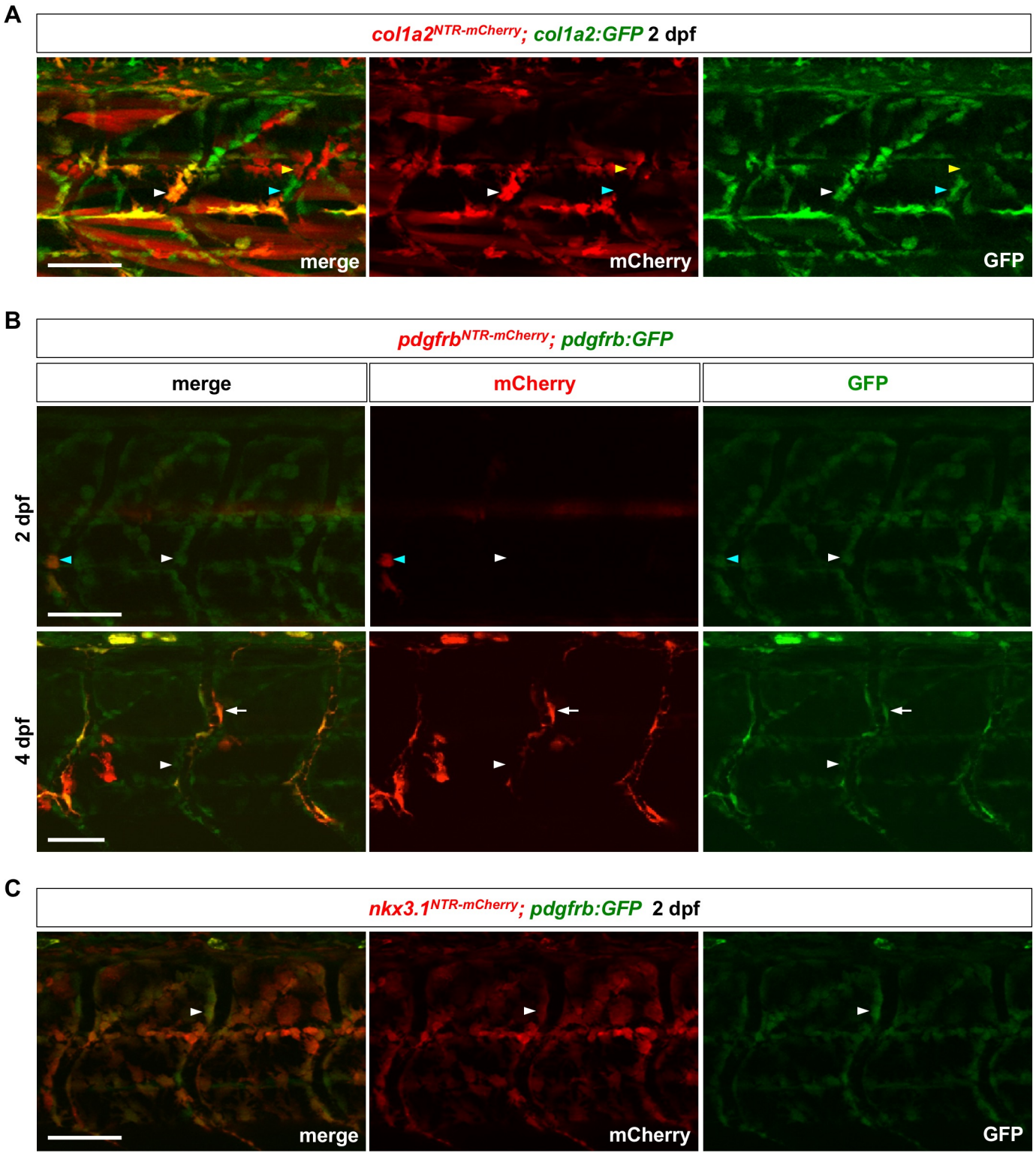
A
col1a2NTR-mCherry; col1a2:GFP 2 dpf
merge
mCherry
GFP
B
pdgfrbNTR-mCherry; pdgfrb:GFP
merge
mCherry
GFP
2 dpf
4 dpf
C
nkx3.1NTR-mCherry; pdgfrb:GFP 2 dpf
merge
mCherry
GFP

Figure S4

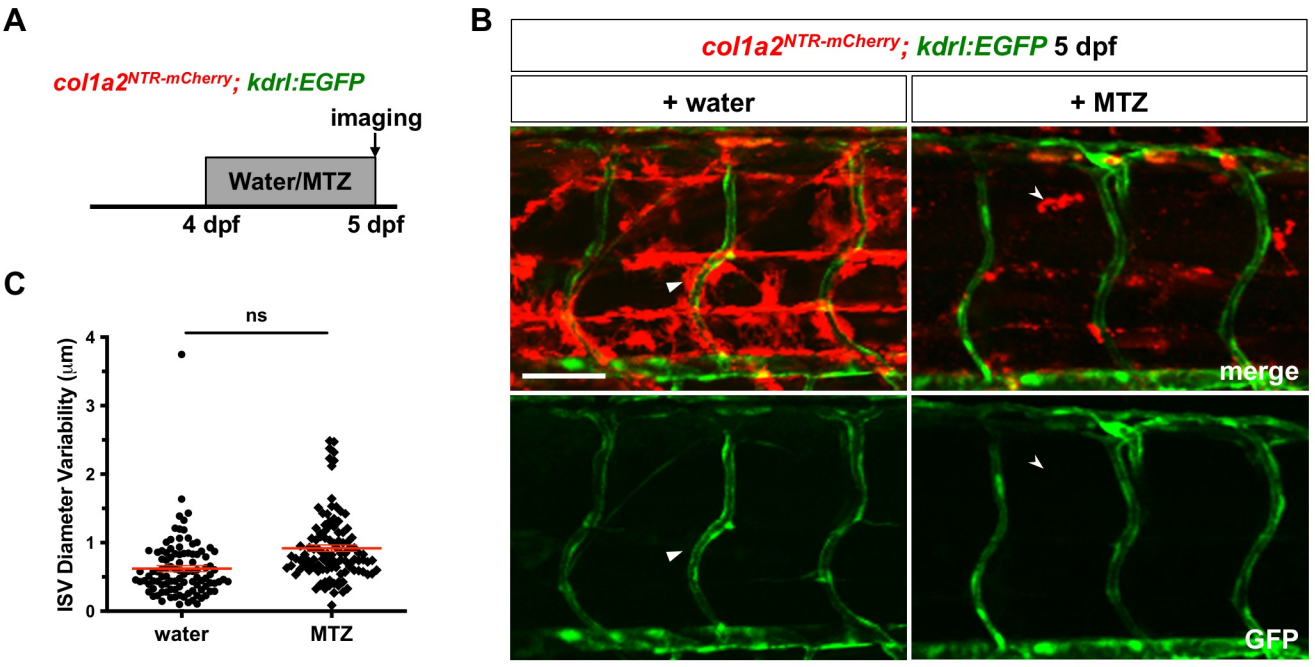
A
col1a2NTR-mCherry; kdrl:EGFP
imaging
Water/MTZ
4 dpf
5 dpf
B
col1a2NTR-mCherry; kdrl:EGFP 5 dpf
+ water
+ MTZ
merge
GFP
C
ns
ISV Diameter Variability (μm)
0
1
2
3
4
water
MTZ

Figure S5

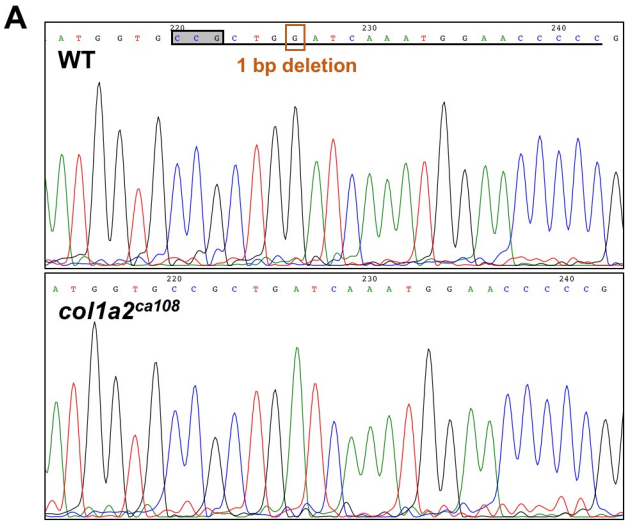

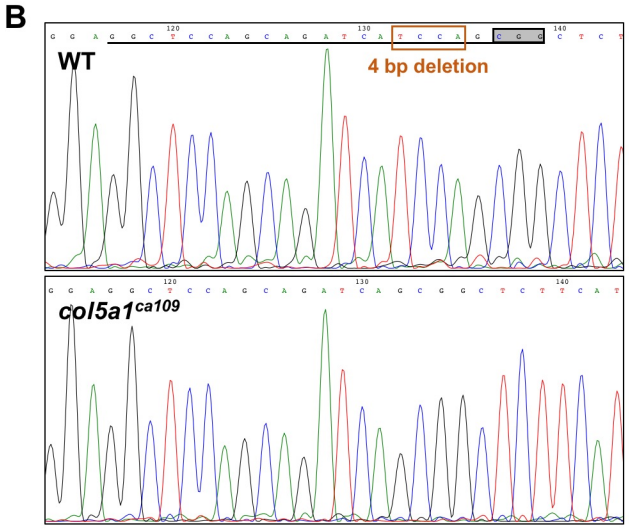

C

```
col1a2_wt       ···GLGGNFAAQYDGAKGPDPGPGPMGLMGPRGPSGSPGAPGAQGLQGHAGEPGEPGQAGAIG  120
col1a2_ca108    ···GLGGNFAAQYDGAKGPDPGPGPMGLMGPRGPSGSPGAPGAQGLQGHAGEPGEPGQAGAIG  120
                   ************************************************************

col1a2_wt          ARGPPGPPGKNGEDGNNGRPGKPGDRGVLGAQGARGFPGTPGLPGMKGHRGYNGIDGRKG  180
col1a2_ca108       ARGPPGPPGKNGEDGNNGRPGKPGDRGVLGAQGARGFPGTPGLPGMKGHRGYNGIDGRKG  180
                   ************************************************************

col1a2_wt          EPGAAGAKGENGAAGSNGTPGQRGGRGLPGER----------------------------  212
col1a2_ca108       EPGAAGAKGENGAADQMEPPDREVVVVFLVREVVLALLAQLVLAVLMVTLVLLALLDLWA  240
                   **************..   *.:.    :  ..

col1a2_wt          --------------GRVGPAGPAG---ARGAD---GNTGPAGPAGPLGSAGP--------  244
col1a2_ca108       QLVLLVSLVHLDPRENLDPLVPLDHLELRDKEESQARTVPLAPLDPLVTLVLMVSMVLKE  300
                                 .:.*  * .    *. :   ..* * .* .** :

col1a2_wt          -PGFPGAPGPKGELGPAGPTGPSGAQGQRGEPGPNGAVGPVGPPGNPGANGINGAKGAG···303
col1a2_ca108       QLVFLELLVPLVSLA------LEEALAHRD------LVE-----------LLVQE----  332
                      *     *  .*.       . * .:*.       *             :   :

col1a2_wt          LPGIAGAPGFPGPRGGPGPQGPSGASGPRGLGGDPGPVGVKGDSGVKGEPGSAGPQGPPG  363
col1a2_ca108       --VLVVTPDLLE-------------------------------------------------  342
                      :. :*.:
```

D

```
col5a1_wt       MFPEDFSILATVRPKKGSQSFLLSVYNEQGIQQLGLEVGRSPVFLYEDHLGKPGPEDYPL  60
col5a1_ca109    MFPEDFSILATVRPKKGSQSFLLSVYNEQGIQQLGLEVGRSPVFLYEDHLGKPGPEDYPL  60
                ************************************************************

col5a1_wt       FRGINLADGKWHRVAISVHKQSITLILDCKKKVTRTLSRSPHPIIDTKGIVVFGTRILDE  120
col5a1_ca109    FRGINLADGKWHRVAISVHKQSITLILDCKKKVTRTLSRSPHPIIDTKGIVVFGTRILDE  120
                ************************************************************

col5a1_wt       EVFEGDIQQLMIVSDHRAAFDYCEHYSPDCEVSAPEQPQNQDPNTDQSNPEEDNYYYEYP  180
col5a1_ca109    EVFEGDIQQLMIVSDHRAAFDYCEHYSPDCEVSAPEQPQNQDPNTDQSNPEEDNYYYEYP  180
                ************************************************************

col5a1_wt       YYEDMDSDKTEETITEETTGTETEVSVPDSGRVITSVISSGSGGSSRSSSGSSSSSSSSS  240
col5a1_ca109    YYEDMDSDKTEETITEETTGTETEVSVPDSGRVITSVISSGSGGSSRSAALHHPLHHHLH  240
                ************************************************::

col5a1_wt       SSSSSSSSSSSSSSNTANTGEDRYDGYDGYDTGYETYYDESTSSPDG-----SRTITITS  295
col5a1_ca109    HHHPPHPLPPPAPTRPIP-----------VRTGMMDMMD---TIPDMKPIMTSRPQVLTA  286
                          : :.               **     *   : **      **  .:*:

col5a1_wt       TGTGSAGELDLGLGEVDHQLGRVDLDRRIITSSSSSSGGEGGTVHSTTTIIRNGTSGSGS···355
col5a1_ca109    --PGPSPSLALVLDQLENWIW----D-------------------------------  306
                   * : .* * *.:::: :     *
```

Figure S6

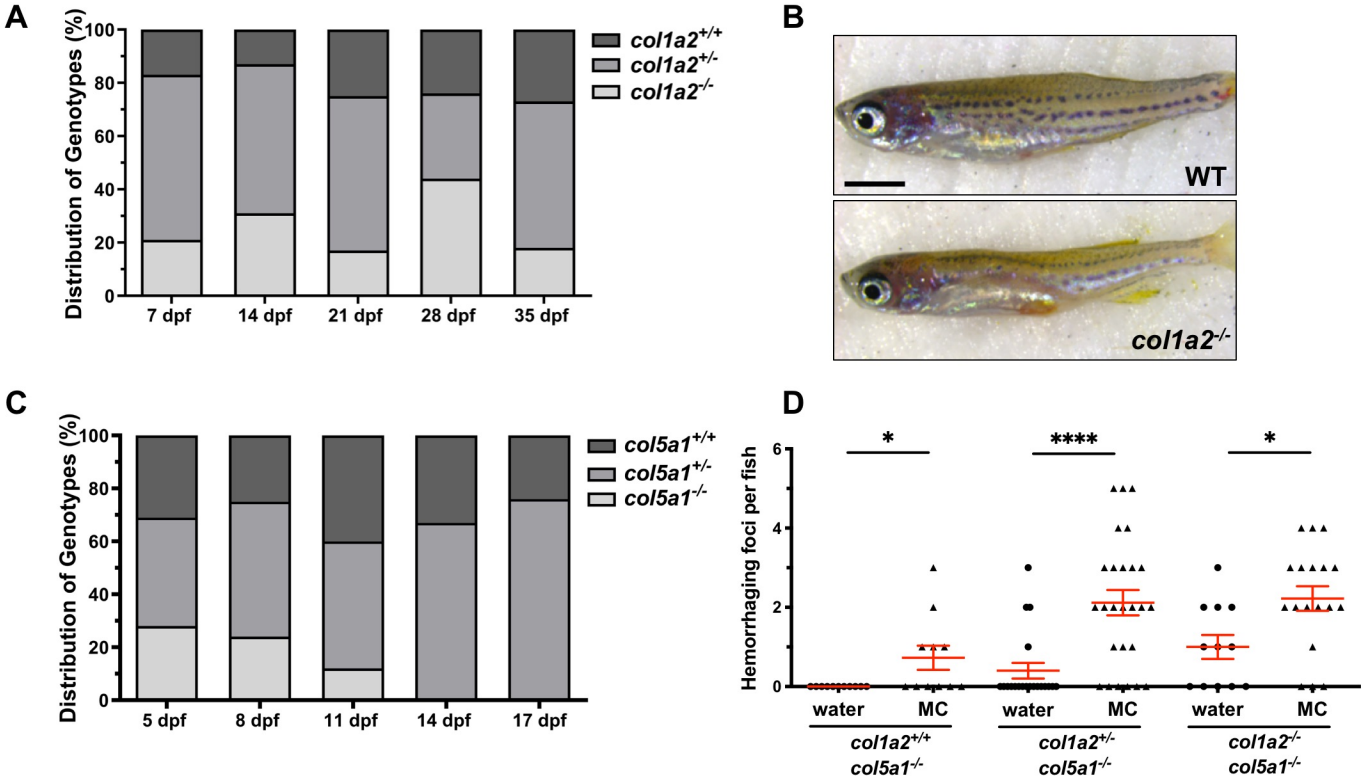
A
Distribution of Genotypes (%)
100
80
60
40
20
0
7 dpf
14 dpf
21 dpf
28 dpf
35 dpf
col1a2+/+
col1a2+/-
col1a2-/-
B
WT
col1a2-/-
C
Distribution of Genotypes (%)
100
80
60
40
20
0
5 dpf
8 dpf
11 dpf
14 dpf
17 dpf
col5a1+/+
col5a1+/-
col5a1-/-
D
Hemorrhaging foci per fish
6
4
2
0
*
****
*
water
MC
water
MC
water
MC
col1a2+/+
col5a1-/-
col1a2+/-
col5a1-/-
col1a2-/-
col5a1-/-